Enzyme Adsorption onto Thin Films of Calcium Phosphate Doped with Titanium

Ana Raquel Carreira Ribeiro

Tese submetida à Faculdade de Engenharia da Universidade do Porto com vista à obtenção do grau de Mestre em Engenharia Biomédica

Faculdade de Engenharia
Universidade do Porto
Abril 2007

This thesis was supervised by:

Professor Doutor Mário A. Barbosa
Faculdade de Engenharia, Universidade do Porto

Doutora Cristina C. Ribeiro
Instituto Superior de Engenharia do Porto

The host institutions of this thesis were:

INEB – Instituto de Engenharia Biomédica, Laboratório de Biomateriais
Universidade do Porto, Portugal

ICEMS – Instituto de Ciência e Engenharia de Materiais e Superfícies, Centro de Engenharia Mecânica, Faculdade de Ciência e Tecnologia
Universidade de Coimbra, Portugal

The research described in this thesis was financially supported by:

Project GAUCHER II - An injectable enzyme delivery system based on apatite nanoparticles and natural hydrogel microspheres for bone regeneration, financed by FCT, POCTI/FCB/41523/2001.

Project PROTEIN - Immobilization of ligands to albumin and thrombin on self-assembled monolayers - influence on thrombus formation and inflammatory reactions, financed by FCT, POCTI/CTM/55644/2004.

Based on the work developed in this thesis the following papers were written:

"Characterization of HAp sputtered films doped with Ti"
A. Ribeiro, A.P. Piedade, C.C. Ribeiro, M.T. Vieira, and M.A. Barbosa
Key Engineering Materials (2006)

"Titanium ions role on GCR enhancement"
A. Ribeiro, C.C. Ribeiro, C.C. Barrias, and M.A. Barbosa
In preparation

Participation in Conferences:

Posters

7th Advanced Course in Cell-Material Interactions
19-23 June 2006, Porto - Portugal
"HSA adsorption on HA films doped with Ti"
A.R., Ribeiro, A.P. Piedade, C.C. Ribeiro, M.T. Vieira, and M.A. Barbosa

Oral presentations

19th International Symposium on Ceramics in Medicine (Bioceramics 19)
"Characterization of HA sputtered films doped with Ti"
A. Ribeiro, A.P. Piedade, C.C. Ribeiro, M.T. Vieira, and M.A. Barbosa

21st European Conference on Biomaterials (ESB 2007)
"Protein adsorption on HA films doped with Ti: evidence for an increased enzyme activity induced by titanium"
A.R., Ribeiro, C.C. Ribeiro, C.C. Barrias, and M.A. Barbosa

To my family,
especially to my nephew

At many times through our lives, we meet people, with which we share, battle, lose and triumph. As any other battle, throughout this last three years, I met amazing people, which believed me, help me, and sometimes, held me, to get there. There, was wherever I wanted, needed or dreamed of.

I want to thank everyone in the road to this point. People touch me in different ways, in different times, with different purposes. And I want to thank you all!! All at INEB!! for being my family during these three years, and hopefully we will be always near by. Everyone at Coimbra!!, for supporting my work, and teaching me so much, many at FEUP, and some from Around…

Some became friends, some became good friends.
But all of us learn things in more than one way, so I want to thank also to the ones who did not cared, or did not noticed, but still made the difference.

I want to express gratitude to friends from others battles (you know who you are, H, I, M, E, B, R, A, L) that continue to support me, as I hope I have been able to support them.

I want to especially thank my supervisor, Professor Mario Barbosa, who believed in me from the beginning; I have a very caring gratitude to my co-supervisor, Doctor Cristina Ribeiro, who also supported me through the work, and who made everything possible and, I believe, the impossible too, to help me get to the end of this journey. I also want to express my gratitude to Professor Maria Teresa Vieira and Doctor Paula Piedade, who so well received me in Coimbra.

The ones I have the most gratitude to are of course my family…
Firstly, I want to thank the newest member of my family, my nephew, Pedrinho, who is a blessing and an inspiration to me; my mother, who always pushes me forward; my father, who supports me at any time, and at any cost; my sister (and my brother in law!), who's advices are always welcome; my grandmothers, who always worries and prays; and a very especial gratitude to my grandfathers João and Manel, who are no longer among us. My "vô" João taught me how to work hard to get what I want, how to be a provider, how to face the sea. My "vô" Manel taught how to be simple, how to dance, how to play cards. They taught me in the end many things that help me to survive in this crazy world.

I live and I change, some change with me, and some do not. At the end, what matters is the journey we made and what we have accomplished …

Abstract

There has recently been an increasing interest in the development of injectable materials for bone regeneration, both ceramic and/or polymer based, via minimally invasive surgery, thus providing less discomfort to the patients and lower costs. In previous works of our group, an injectable system was developed in the form of ceramic based microspheres of calcium titanium phosphate (CTP) to be used as bone regeneration scaffolds and enzyme delivery systems. It was shown that CTP could in specific applications have a better performance then hydroxyapatite (HA), a traditional calcium phosphate used in orthopedic applications. For instance in what concerns the immobilization of the enzyme glucocerebrosidase (GCR), CTP adsorbed a much higher amount of GCR per unit surface area than HA, and a higher catalytic efficiency of the enzyme was observed when CTP was used as a substrate. Nevertheless, the role of titanium ions in biological processes such as cell adhesion and protein adsorption is a subject that is not completely understood and needs further investigation.

In the present work, films of HA, Ti and HA doped with titanium were obtained, characterized, and used as model surfaces for human serum albumin (HSA) and GCR adsorption studies.

Thin films of HA, Ti and HA doped with different titanium concentrations, ranging from 8 to 26% (atomic %), were sputtered on gold and steel substrates. The films were characterized using different techniques namely electron probe microanalysis (EPMA), X-ray diffraction (XRD), X-ray photoelectron spectroscopy (XPS), Fourier Transform Infrared Spectroscopy (FTIR), contact angle measurements, Atomic Force Microscopy (AFM) and Zeta potential (ZP). The adsorption of HSA (control) and GCR to the substrates was quantified by radiolabelling, according to the iodogen method. The GCR catalytic activity upon adsorption was evaluated as the hydrolysis of 4-MU-β-d-glucopyranoside. FTIR (IRAS) and AFM analysis was also performed to complement the adsorption studies.

The microprobe analysis showed that the Ca/P ratio of the HA films was higher than 1.67, indicating the presence of CaO as a secondary phase. It was also observed that the Ca/P ratio increased with the Ti content, suggesting that there is a competition between Ti and P in the deposition process and/or P is being ejected from the film by other incoming atoms. X-ray diffraction analysis showed that all sputtered thin films were amorphous. After heat treatment

only the crystallinity of HA films was increased, indicating that the presence of Ti destabilizes the HA lattice inhibiting its crystallization. FTIR results were in agreement with these observations. An increase in the Ti percentage of the films resulted in the broadening of the characteristic phosphate bands in the FTIR spectra. XPS analysis indicated that for a concentration in Ti of 26 at.%, a Ti-P rich phase is obtained. Wettablility studies showed that the contact angle of the films ranged from 85º to 102º. In what concerns surface morphology, AFM analysis indicated that the insertion of Ti in the ceramic films lead to smoother surfaces when compared to HA films.

HA-Ti doped films adsorbed less HSA and GCR per unit surface area than HA. The presence of Ti in the substrate significantly enhances the activity of the enzyme GCR.

The results obtained indicate that titanium ions significantly influence protein adsorption and supports previous suggestion of our group that a titanium-rich calcium phosphate may be used as a delivery matrix for biologically active molecules, in particular GCR.

Resumo

Recentemente, tem existido um interesse crescente no desenvolvimento de materiais injectáveis para regeneração óssea, com base cerâmica ou polimérica, através de cirurgias pouco invasivas, proporcionando menos disconforto ao paciente e menores custos. Em trabalhos anteriores do nosso grupo, foi desenvolvido um sistema injectável sob a forma de microesferas de fosfato de cálcio e titânio (CTP), para ser utilizado como uma matriz de regeneração óssea e como um sistema de libertação de enzimas. Foi demonstrado que o CTP pode, em aplicações específicas, ter um melhor desempenho do que a hidroxiapatite (HA), um fosfato de cálcio tradicionalmente utilizado em aplicações ortopédicas. Por exemplo, no que diz respeito à imobilização da enzima glucocerebrosidase (GCR), o CTP adsorve uma maior quantidade desta enzima por unidade de área superficial do que a HA e uma maior eficiência catalítica da enzima foi observada aquando da utilização do CTP como substrato. No entanto, o papel dos iões de titânio nos processos biológicos, tais como a adesão celular e a adsorção proteíca, é um assunto que não está completamente compreendido e necessita de ser mais investigado.

No presente trabalho, filmes de HA, Ti e HA dopado com titânio foram obtidos, caracterizados e utilizados como superfícies modelo para estudos com Albumina de Soro Humano (HSA) e GCR.

Filmes finos de HA, Ti e HA dopada com diferentes concentrações de titânio, compreendidas entre 8 e 26% (% at.), foram pulverizados sobre substratos de aço e ouro. Os filmes foram caracterizados usando diferentes técnicas nomeadamente microsonda (EPMA), difracção de raios-X (XRD), espectroscopia electrónica de raios-X (XPS), Espectroscopia de Infravermelhos com Transformada de Fourier (FTIR), medição de ângulos de contacto, Microscopia de Força Atómica (AFM) e Potencial Zeta (ZP). A adsorção de HSA (controlo) e de GCR aos substratos foi quantificada pela técnica de marcação de moléculas com isótopos radioactivos, de acordo com o método do Iodogénio. A actividade catalítica da GCR após adsorção foi avaliada com base na a hidrólise de 4-MU-β-d-glucopiranósido. Os estudos de adsorção foram complementados com análises de FTIR (IRAS) e AFM.

A análise por microsonda demonstrou que a razão Ca/P dos filmes de HA era mais elevada do que 1.67, indicando a presença de CaO como fase secundária. Também

foi observado que a razão Ca/P aumentou com o teor de Ti, sugerindo uma competição entre o Ti e o P no processo de deposição e/ou que o P está a ser ejectado do filme por outros átomos. A análise por difracção de raios-X demonstrou que todos os filmes finos depositados eram amorfos. Após um tratamento térmico apenas a cristalinidade dos filmes de HA aumentou, indicando que a presença do Ti destabiliza a rede da HA inibindo a sua cristalização. Os resultados de FTIR estão de acordo com estas observações. Um aumento da percentagem de Ti nos filmes resultou num alargamento das bandas de fosfato no espectro do FTIR. A análise por XPS indicou que para concentrações de Ti superiores a 26% (% at.), uma fase rica em Ti e P é obtida. Estudos de molhabilidade mostraram que o ângulo de contacto dos filmes variou entre 85 e 102Âº. No que diz respeito à morfologia da superficie, as análises por AFM indicaram que a inserção do Ti nos filmes cerâmicos originou superfícies menos rugosas quando comparadas com os filmes de HA.

Os filmes dopados HA-Ti adsorveram uma menor quantidade de HSA e GCR por unidade de área superficial do que os filmes de HA. A presença de Ti no substrato aumentou significativamente a actividade da enzima GCR.

Os resultados obtidos indicam que os iões de Ti influenciam significativamente a adsorção de proteínas e apoiam resultados prévios obtidos pelo grupo de que um fosfato de cálcio rico em titânio pode ser utilizado como uma matriz de libertação de moléculas biologicamente activas, em particular GCR.

Contents

Chapter I

Chapter II

Chapter III

Chapter IV

Index of Figures

Chapter II

Chapter III

Index of Tables

Chapter I

Chapter II

Chapter III

1. Injectable Bone Substitutes

A large number of orthopaedic procedures are performed each year due to traumas, birth defects, infections, and tumours [1-4]. Such cases may create defects in the skeleton that need to be filled [4]. Conventional treatment of bone traumas involve the removal of the dead tissue, followed by repeated surgeries for irrigation of the wound and long term antibiotics administration. Sometimes, amputation is needed. The alternative implies the use of naturally derived substitute materials or synthetically produced ceramics [3-8], and can involve growth factors, cytokines, gene therapy, and tissue engineering [1]. Most bone tissue engineering strategies are supported by the use of temporary scaffolds, which can be seeded with cells before implantation, or designed to induce bone formation after implantation [9, 10]. The increasing interest in this procedure is translated in developing new materials which are injectable and biodegradable, avoiding open surgeries, improving comfort and less pain to the patient [11, 12]. For that reason, injectable bone substitutes (IBS) are being developed with the aim of acting as bone fillers, and of providing faster bone healing [12-14].

1.1 Injectable Bone Substitutes materials

Several materials have been developed to be applied as injectable bone substitutes. Most of them are ceramics or polymer based materials. The first include synthetic ceramics such as hydroxyapatite, tricalcium phosphate, carbonated hydroxyapatite, calcium sulphate, natural ceramics such as coral, and ceramic cements. The second group comprises bio-resorbable natural and synthetic polymers [13, 15-17]. These materials are available in pastes, gels or liquid precursors which solidify *in situ* after being implanted [11, 14, 18]. One of the most commonly used injectable bone substitute is poly(methyl methacrylate) (PMMA), but it suffers from the fact that it is not degraded and that its high curing temperatures can cause necrosis of the surrounding tissue [11]. Therefore, bone substitutes are needed and alternative ceramics are currently under investigation.

1.1.1 Hydroxyapatite

Hydroxyapatite (HA) is the main component of teeth and bones in vertebrates [19] and, as bone mineral, it constitutes approximately 5% of the body weight and provides storage for control of calcium uptake and release [20]. HA is also the major component of the bone mass (65%), being the remaining organic matter (most of it collagen) and water. It is the essential crystalline part of the calcified components of the skeleton and is the principal mineral in bone, enamel, dentin, and cement [21].

Hydroxyapatite is the ceramic most used as a biomaterial for bone substitution or implant coating. It is especially useful in the dental and orthopaedic fields [20, 22].

Hydroxyapatite ceramics do not exhibit cytotoxic effects, show excellent biocompatibility with hard-tissues and also with skin and muscles tissues [21].

1.1.1.1 Biological Hydroxyapatite

Bone and tooth apatites are called biological apatites. Other biological apatites are seen in large or small quantities in pathological calcified tissues including salivary stones, urinary stones, etc. Biological apatites exist in small interstitial spaces in the linear chains of bone fibbers, in a controlled biomineralization process involving more than 200 different acid proteins. These proteins act as inhibitors, nucleators or templates for the epitaxial growth of nanocrystals, anchored to the collagen [20].

1.1.1.2 Synthetic Hydroxyapatite

Hydroxyapatite has been produced synthetically since early 1970s and has been used clinically since 1980s [21]. Generally, different synthetic types of calcium phosphate have Ca/P ratios ranging from 2.0 to 0.5, and can be synthesized by mixing a calcium and phosphate ion solution under acid or alkaline conditions [20]. The crystallization of the complex and hardly soluble apatite structures evolves favourably through the kinetically controlled formation of metastable intermediate products [22]. The different Ca/P ratios have a direct relation with the acidity and solubility of the mixture. The lower the ratio the larger the acidity and the higher solubility of the compound. The Ca/P ratio is a very useful parameter for scientists working in this field, as it differentiates the various calcium phosphates [22].

1.1.1.3 Sintered Hydroxyapatite

The early hydroxyapatite implants were sintered, which is a process that causes crystals to rearrange by heating them at elevated temperatures (more than 500ºC) [21]. Sintering leads to an increase of mechanical resistance. As the temperature of sintering increases there are various properties that also increase, such as: density, grain size, compressive, flexural, torsional and dynamic strength, and the modules of elasticity in compression and bending [19]. The main applications of sintered hydroxyapatite in the biomedical field include reinforcement in composites, coatings and granular fill for direct incorporation into human tissues [23].

1.1.1.4 Hydroxyapatite structure

Hydroxyapatite is a stoichiometric compound, which accepts compositional variations in its three sublattices. The chemical formula is represented as [20]:

$$Ca_{10}(PO_4)_6(OH)_2$$

The formula for bone apatite is not exact and, in fact, the chemical compositions of bone apatites are slightly different according to species, ages, and parts of the skeleton [18].

1.1.1.5 Hydroxyapatite Properties

Bones can exhibit different types of integration between organic and inorganic matter, leading to significant variations in their mechanical properties [22]. Stoichiometric hydroxyapatite (bulk Ca/P ratio 1.67) has been shown to have a negative charge through zeta potential measurements of powder suspensions with granule sizes comprised between 5–50 μm [19].

Hydroxyapatite is being investigated in a wide variety of forms for use in different bone implant applications [19]. The different products on the market have been applied in many different locations and have promoted bone ingrowth and healing of the defects [13]. The nanoscale surface chemical properties (e.g. surface functional groups, charge distribution), and morphological structure (e.g. grain size, shape, distribution, roughness) will significantly influence the implant's interaction with the biological environment, and how the implant performs *in vivo* [19]. Nevertheless, questions concerning the effects of small crystallites on fracture healing, the addition of growth

factors or antibiotics to the *in situ* setting materials, and other physical-chemical and biological properties still have to be addressed in future studies [13, 20].

1.2 Injectable Bone Substitutes properties

The mechanical properties of the material to be implanted must be as similar as possible to those of the tissue that is to be repaired or regenerated. This is especially important in the initial mechanical properties, which provide proper support in the early stages of healing, and in the graded load transfer needed later in the process of creation of replacement tissue. Tissue formation will be promoted depending on the amount of void space and degradation time of the biomaterial, so these properties must be chosen to promote tissue growth and vascularization, when needed. The degradation rate matched with the rate of tissue formation, are ideal for the non-compromising load-bearing capabilities of the tissue [11].

Infections are major risks in surgeries, and sterilization of the materials to be used is crucial. The material must be chosen so as to be easy to sterilize, without interfering with its bioactivity or altering its chemical composition, which in turn affect its compatibility and degradation properties [11]. The setting time should be established in a way to minimize the length of the procedure, but allowing time for the surgeons to place the material before hardening [11]. This parameter is also related with the inflammatory response, as shown by the fact that CaP with long setting time resulted in a profound inflammatory response, while fast setting cements showed significantly less tissue reaction [15]. If the setting reaction involves a temperature change, the increase or decrease should be as small as possible to reduce damage to the surrounding tissue [11]. Ease of handling is of utmost importance for clinical use of any biomaterial. Both ceramic-based and polymer-based biomaterials already existing in the market fulfil the need of the material to remain at the site of injection, and the need for the surgeon to easily manipulate its placement [11]. Rheological properties must be suitable to ensure bonding of the mineral phase *in situ* with good cell permeability, while intrinsic porosity is required to provide rapid and deep bone formation [12, 17]. The stable composition and properties of the biomaterials must be suitable for the reproductibility of the biological response [12].

The results of the injectable biomaterials developed until now are promising and lead the way for a new era of orthopaedic materials that provide more and better tissue regeneration [11], convenient for filling complex-shaped bone defects using arthroscopy [4, 17].

1.3 Injectable Bone Substitutes as Drug Delivery Systems

The effectiveness of injectable bone substitutes can be highly improved if they can act simultaneously as drug delivery systems [14, 24, 25].

Controlled drug delivery is a major subject in biomaterials research. Many mechanisms have been studied and a wide variety of applications are envisaged. Several approaches can also be used to better control the release profile needed, with different carriers, like micelles, vesicles, multifunctional dendritic polymers, liquid crystals, or nano and microspheres [26].

Ceramic bone substitutes can be loaded with growth factors, protein or antibiotics [13]. In fact, the incorporation of osteogenic factors would increase their potential as bone regeneration materials [4]. With degradation or resorption of the ceramic, the added drug is slowly and continuously released into the surrounding tissues. This behaviour will enhance fracture healing and reduce infection or inflammation [13]. Since 1990, Aoki and his colleagues have been using hydroxyapatite microcrystals as drug carriers for growth restriction of cancer cells and HIV [20]. Different ceramic compositions give rise to different resorption times and a wide range of drug release kinetics in the body [13].

Drug delivery systems are generally classified in three types depending on the mechanism by which the drug is released: a) devices controlled by diffusion, b) devices controlled by chemical processes, and c) devices controlled externally. In devices controlled by diffusion, the drug is incorporated into a non-biodegradable matrix, or is surrounded by a stable membrane through which it should diffuse. The release kinetics will be dependent on the diffusion process through the matrix or the membrane outwards. In devices controlled by chemical processes, the drug is introduced in a biodegradable matrix. The release kinetics is related to the kinetics of matrix degradation [4]. The latter type of devices is controlled externally and/or electronically. Delivery system models are being developed to respond to mechanical signaling, such

as temperature, pH, ultrasound, and electric or magnetic field, and upregulate the release of the drug. As most tissues in the body are subjected to mechanical stimuli, signalling should be considered in the design of polymeric matrices that release growth factors [24].

Synthetic and naturally derived polymers and ceramic materials can be used similarly as storage and delivery vehicles of protein growth factors [24, 26]. In this way, drug delivery systems will increase the efficiency of bone treatment. For example, the advantage of a release system of antibiotic in the treatment of osteomyelitis goes through the maintenance of a localized increase of the drug and thus a more effective control of bacterial and fungal growth [26].

1.3.1 Ceramic based Injectable Systems developed at INEB

In previous work of our group injectable ceramic and ceramic-alginate microspheres were developed, which are intended to be used as enzyme delivery matrices and bone regeneration templates [4, 27]. In what concerns the ceramic phases, calcium-titanium phosphate (CTP) was used as well as HA. Studies were performed on the ability of CTP-alginate and HA-alginate microspheres to act as carriers for Glucocerebrosidase (GCR) [4, 28, 29]. This specific enzyme was chosen due to the fact that our research group was involved in a project aiming at developing an enzyme delivery system to be used in patients with bone lesions associated to Gaucher disease. It was observed that CTP adsorbed a much higher amount of enzyme per unit area than HA. Further studies from our team also showed that while in the presence of HA there is some degree of inactivation of GCR, in the presence of CTP a much higher catalytic efficiency was observed. Also, cell culture investigations support the applicability of CTP microspheres as scaffolds for bone tissue regeneration since bone marrow stromal cell are able to attach, spread, and grow on the surface of CTP microspheres [29-31].

Although the results obtained until now clearly support the interest in the use of CTP as an alternative ceramic to the traditional calcium phosphates for orthopaedic surgery, the role of titanium ions in biological processes such as protein adsorption is a subject that is not completely understood and needs further investigation.

2. The Model System used for protein adsorption studies

Sputtering is a very versatile and widely used deposition technique [32] that allows to obtain thin coatings with good adherence, smoothness and density [33, 34]. Using this technique it is possible to produce films with a uniform structure and a composition tailored according to a required stoichiometry. Taking this into account, sputtering was chosen as the deposition technique to prepare thin films of HA doped with different Ti contents to be used as a model system in protein adsorption studies.

3. Proteins and enzymes

3.1 Definition

Proteins are molecules composed of one or more polypeptides, and each peptide is composed of many amino acids regularly linked by peptide bonds into long chains. Each protein has its unique amino acid sequence and composition, genetically determined.

Proteins are incomparable in being able to recognize and bind a remarkably diverse array of molecules. Proteins determine the pattern of chemical transformations in biological systems by catalyzing nearly all the necessary chemical reactions [35].

3.2 The basic unit of proteins

Amino acids are the basic structure units of proteins, from bacteria to humans. Proteins are built from a collection of twenty of these basic structures, as described in Table 1 [36, 37].

Table 1. List of the twenty amino acids, their respective abbreviations, molecular weight and pI [36]. * Amino acids which contain sulfur. ** Amino acids which can be phosphorylated [37].

Name	Abbr.		Linear structure formula	Mol Wt	pI
Alanine	Ala	a	CH_3-CH(NH_2)-COOH	89.09	6.00
Arginine	Arg	r	HN=C(NH_2)-NH-$(CH_2)_3$-CH(NH_2)-COOH	174.20	11.15
Asparagine	Asn	n	H_2N-CO-CH_2-CH(NH_2)-COOH	132.12	5.41
Aspartic acid	Asp	d	HOOC-CH_2-CH(NH_2)-COOH	133.10	2.77
Cysteine*	Cys	c	HS-CH_2-CH(NH_2)-COOH	121.15	5.02
Glutamine	Gln	q	H_2N-CO-$(CH_2)_2$-CH(NH_2)-COOH	146.15	5.65
Glutamic acid	Glu	e	HOOC-$(CH_2)_2$-CH(NH_2)-COOH	147.13	3.22
Glycine	Gly	g	NH_2-CH_2-COOH	75.07	5.97
Histidine	His	h	NH-CH=N-CH=C-CH_2-CH(NH_2)-COOH |_____|	155.16	7.47
Isoleucine	Ile	i	CH_3-CH_2-CH(CH_3)-CH(NH_2)-COOH	131.17	5.94
Leucine	Leu	l	$(CH_3)_2$-CH-CH_2-CH(NH_2)-COOH	131.17	5.98
Lysine	Lys	k	H_2N-(CH)4-CH(NH_2)-COOH	146.19	9.59
Methionine*	Met	m	CH_3-S-$(CH_2)_2$-CH(NH_2)-COOH	149.21	5.74
Phenylalanine	Phe	f	Ph-CH_2-CH(NH_2)-COOH	165.19	5.48
Proline	Pro	p	NH-$(CH_2)_3$-CH-COOH |_____|	115.13	6.30
Serine**	Ser	s	HO-CH_2-CH(NH_2)-COOH	105.09	5.68
Threonine**	Thr	t	CH_3-CH(OH)-CH(NH_2)-COOH	119.12	5.64
Tryptophan	Trp	w	Ph-NH-CH=C-CH_2-CH(NH_2)-COOH |_____|	204.23	5.89
Tyrosine**	Tyr	y	HO-p-Ph-CH_2-CH(NH_2)-COOH	181.19	5.66
Valine	Val	v	$(CH_3)_2$-CH-CH(NH_2)-COOH	117.15	5.96

Amino acids vary in size, shape, charge, hydrogen-bonding capacity and chemical reactivity to form different proteins. A chain of amino acids linked together through peptide bonds forms a protein [35-37].

3.3 Proteins structure

Proteins consist of strands of amino acids joined together by peptide bonds to form a polypeptide chain. The biological function of a protein depends on its conformation, characterized by the three-dimensional arrangement of the atoms of a molecule folded into a particular shape. The different protein structures can be classified in four basic levels of structure depending on the complexity of the folding. Primary structure is the amino acid sequence, the very basic strand of amino acids. Secondary structure is characterized by the hydrogen-bon interaction among strands of amino acids, giving rise to the first level of folding. In this structure a spatial arrangement of amino acids residues takes place and alpha-helices and beta-sheets are formed. Tertiary structure is regarded as the rearrangement of amino acids residues far apart in the linear sequence. There is an interaction between the alpha-helices and the beta-sheets previously formed. Proteins form small globular subunits at this folding level. Quaternary structure refers to the spatial arrangement and the nature of the contact between the subunits, forming protein aggregates. A well-known example of this kind of structure is Hemoglobin, which consists of two α and β chains [35, 38].

Many amino acids may be modified after synthesis of a polypeptide chain to enhance its capabilities. For example, acetylation may occur at the ending part of proteins, making these proteins more resistant to degradation. Conformational changes transmitted between distant sites in protein molecules are at the heart of the capacity of proteins to transduce energy and information [35, 38].

3.4 Proteins function

Proteins are vital players in virtually all biological processes. Their impact and the amazing capacity of their activity comports diverse functions.

Once nearly all known enzymes are proteins, proteins are essential in determining the pattern of chemical transformations in biological systems. Some of these are relatively simple, and others highly complex. Normally, chemical transformations proceed at perceptible rates in the absence of enzymes. With these enzymes reaction rates increase by at least a million fold. The catalytic power of enzymes comes from their capacity to

bind substrates in particular orientations and to stabilize transition states in the making and breaking of chemical bonds [35].

Numerous small molecules and ions are transported by specific proteins. For example, haemoglobin transports oxygen in erythrocytes. Iron is carried in the plasma of blood by transferrin and is stored in the liver as a complex with ferritin, a different protein [45].

Proteins are also important in the coordinated motion, since proteins are the major component of muscle. The sliding motion of two kinds of proteins filaments produces the muscle contraction. Another example of proteins motion function is the movement of chromosomes in mitosis, produced by contractile assemblies consisting of proteins [35].

The mechanical support given by the high tensile strength of skin and bones is due to the presence of a fibrous protein, collagen [35].

Another function is specificity, which relates with immune response. Antibodies are highly specific proteins that recognize and combine with foreign substances, playing a vital role in organisms' immune protection [35].

The response of cells to specific stimuli is mediated by receptor proteins responsible for generating and transmitting nerve impulses [35].

In higher organisms growth and differentiation are controlled by growth factor proteins, and many hormones are proteins. They can also control growth and differentiation of cells [35].

3.5 Enzymes

Enzymes are molecules with catalytic power and specificity. Nearly all enzymes are proteins. Enzyme catalytic activity speeds up or slows down reactions; however they do not alter reaction equilibrium. Enzymes determine the pattern of chemical transformations, and mediate the transformation of different forms of energy. The catalysis of reactions is possible due to stabilization of the transition states. These molecules bring substrates together in an optimal orientation and then make or break chemical bonds. The substrates are bound to a specific region of the enzyme called the active site, which contains residues, catalytic groups, which directly participate in the making or breaking of bonds. Enzymes can also act as molecular switches in regulating

catalytic activity and transforming energy due to their capacity to couple actions of separate binding sites [35].

An enzyme usually catalyzes a single chemical reaction or a set of closely related reaction, and each enzyme acts on a specific substrate. The substrate is the reactant that the enzyme will act upon. Substrate is converted into different molecules named reaction products. The catalytic cycle begins when the substrate enters the active site, forming the enzyme-substrate complex. Upon enzymatic reaction, products are release and the enzyme remains intact, ready to accept another substrate molecule [35].

Some enzymes need supplementary components to denote activity, called cofactors. Cofactors can be either inorganic, like metal ions, or organic compounds, like flavin [35].

Beyond these mechanisms, enzymes are controlled by different molecules and means. Inhibitors are molecules that decrease enzyme activity, while activators increase its activity. In a biosynthetic pathway, feed-back inhibition may occur. This inhibition takes place at the first step in the pathway, and is promoted by the final product, when it reaches a sufficiently high level. When the level of the same product drops sufficiently, the enzyme becomes active again, and continues synthesizing. Enzymes are also controlled by regulatory proteins, stimulating or inhibiting catalysis. Moreover, enzymes can be inhibited by specific molecules and ions, some of them drugs and toxic agents. The inhibition can be reversible or irreversible. In reversible inhibition, inhibitors may be competitive and non-competitive. While the competitive ones compete for the active site of the enzyme, the non-competitive bind in a regulatory site, which in turn changes the active site shape [35].

As in proteins, certain modifications, such as phosphorylation of some amino acids or proteolytic activation may modulate enzymatic activity [35].

Enzymes are of major importance in metabolism as intervene in molecules degradation, being crucial in metabolic cycles.

4. Experimental Techniques

4.1 Thin films preparation

Sputtering is a deposition technique that allows the production of different types of coatings on several substrates. It involves three steps: the bombardment of the coating material with energetic particles; the ejection of the material atoms by exchange of the quantity of movement; and the deposition of the ejected species onto the substrate [39]. In this technique gas plasma (argon, neon, krypton or xenon) is used to remove material from a negatively charged target and to deposit it as a thin film coating onto a substrate [40]. Radiofrequency (RF) magnetron sputtering consists of a magnet on the target side, which increases the efficiency of the sputtering process.

In the biomedical field, sputtering is normally used to coat titanium implants (dental implants and artificial joints) with calcium phosphates [41-43]. Thian et al. emphasizes that this deposition technique preserves Ti mechanical properties while maintaining the bioactivity of the coated HA [44]. It is also known that sputtered CaP coatings promote the differentiation and expression of osteogenic cells, and that bone formation proceeds faster on CaP coatings than on Ti implants without the coating [33, 34, 44, 45]. Wolke *et al.* also demonstrated that magnetron-sputtered CaP coatings can stimulate extracellular matrix and induce apatite formation [46].

Sputtering technique has the advantage of being able to produce thin films with uniform structure, strongly adhered to the substrate, even if it has a complex geometry [44, 46, 47]. Moreover, since the substrate temperature during the deposition can be kept low, the method is also suitable for the deposition on polymers [33]. However, this technique produces amorphous films and, when multi-elemental compounds targets are used, non-stoichiometric depositions take place [48].

4.2 Films characterization

Several techniques were used to characterize the model chosen, especially what relates to the surface properties of the films, which is of utmost important when a biomaterial contacts living tissue.

4.2.1 X-ray Photoelectron Spectroscopy (XPS)

The X-ray photoelectron spectroscopy is an electron spectroscopy, as it measures electron properties. The sample to be analysed is placed in a vacuum environment and irradiated with photons [49]. The interaction of the X-rays with the atoms in the specimen causes the emission of a core level electron [50]. The emitted electrons are separated according to energy and counted. The energy of the photoelectrons is related with the atomic and molecular environment from which they originated [49, 50]. This technique gives qualitative and semi-quantitative information of all elements present, providing information about chemistry, organization, and morphology of a surface [49]. Its measurements can reach 10-250 Å depth, with a spatial resolution between 10-150 μm, and an analytical sensitivity of 0.1 at% [50].

The advantages of this method include the high information content, the surface localization of the measurement, the speed of analysis, the low damage potential, and the ability to analyze most samples with no specimen preparation. The disadvantages include the need for vacuum compatibility (particularly important for hydrated specimens), the possibility of sample damage by X-rays if long analysis times is used, the need for experienced operators, and the cost associated with the complex instrumentation [50].

When analyzing a sample, first, a wide scan is made in which the energies of all emitted electrons over, typically, a 1000 eV range are detected. Then, narrow scans are made in which each of the elements detected in the wide scan is examined with higher resolution. From the wide scan we learn the elements that the specimen contains. The narrow scan is done to each element and shows the shape of the peak and its position indicating the type of bonding that may exist [50].

4.2.2 Fourier Transform Infrared – Infrared Reflection Absorption Spectroscopy (FTIR – IRAS)

The FTIR technique is a powerful method to obtain relevant information about a surface, but also offers a unique mean to understand protein adsorption to surfaces [51]. The infrared radiation is absorbed and excites molecular vibrations. This spectroscopy provides information on the vibrations of atomic and molecular species. It is a standard analytical method that can reveal information on composition, and molecular chemical bonds, specific chemistries, crystallinity, and molecular orientation [50]. Infrared Reflection Absorption Spectroscopy (IRAS) is a sampling mode from the three offered by FTIR [50] that has been widely applied to self-assembled monolayers (SAMs), but is applicable to many surface films. The surface where thin films are upon must be highly reflective and metal surfaces work best [50]. This mode is widely used for studying proteins adsorbed to surfaces through air [51].

It has a depth analysis of 1-5 μm, a special resolution of 10 μm, and an analytical sensitivity of 1 mol% [50].

4.2.3 Contact Angle Measurement

The contact angle technique is based on the three-phase equilibrium which occurs at the contact point at the solid/liquid/vapour or solid/liquid/liquid interface [52]. The contact angle phenomenon can be explained as a balance between the force with which the molecules of the liquid (in the drop) are being attracted to each other (a cohesive force) and the attraction of the liquid molecules for the molecules that make up the surface (an adhesive force). When equilibrium is established between these forces the energy is minimum. The force balance between the liquid-vapour surface tension of a liquid drop and the interfacial tension between a solid and the drop is manifested through the contact angle of the drop with the surface. This contact angle can be used to quantitatively characterize the energy of the surface [50]. This equilibrium is normally considered in terms of the surface and interfacial tensions or surface and interfacial free energies present [52].

There are various methods of measuring the contact angle, being the measurements of the dimensions of a drop profile on a surface the one mostly described. In this

measurement, contact angle can be calculated through spherical trigonometric relationships, [52].

In contact angle measurements liquid wetting of surfaces is used to estimate the energy of surfaces. This technique also allows the determination of the affinity of specific biomolecules (such as proteins) to a surface, by the calculation of the adhesion work. It reaches a depth of 3-20 Å, with a spatial resolution of 1 mm, and the analytical sensitivity depends on the chemistry of the surface. Contact angle methods are inexpensive, and provide a "first line" of materials characterization [50].

4.2.4 X-Ray Diffraction (XRD)

X-ray diffraction is a versatile and non-destructive technique for the identification of the crystallinity and crystalline phases of the sample components. It gives structural information about order at surfaces and interfaces by the comparison of a XRD model with the unknown sample [50]. A crystalline sample has its atoms distributed in parallel plans, separated with a certain distance. When a beam of X-ray with a given wavelength goes through the network the diffraction occurs, giving the regular positions and the intensities from the diffraction peaks, which characterizes the sample. If a sample is amorphous no peaks appear [53].

4.2.5 Electron Probe Microanalysis (EPMA)

Electron microprobe analysis is a microanalysis technique ideal for materials characterization, which uses a focused beam of high energy electrons (5 - 30 KeV) to non-destructively ionize a solid specimen surface for inducing emission of characteristic X-rays (0.1 - 15 KeV) [54]. This technique is used for high accuracy elemental characterization on the micro (bulk samples) and nano scales (thin films) [54], for major (500-1000 ppm), minor and trace element concentrations (near 20 ppm) [55]. They can provide qualitative and quantitative information for Be to U and also X-ray, secondary, backscatter and cathodo-luminescence imaging [55].

This technique is used to obtain chemical data and images that show the distribution and variation of materials constituents. The technique combines high sensitivity (~0.01 wt % detection limit), high speed (seconds to minutes per analysis), high precision and accuracy (1-2 % errors), and high spatial resolution (0.001mm analysis area). The

spatial resolution of X-ray microanalysis of thick specimens is limited to a volume with dimensions of approximately 1 micrometer due to electron scattering effects. Spatial distribution of elemental constituents can be visualized quantitatively by digital composition maps and displayed in grey scale or false colour [55].

This analytical approach is widely used in chemical distribution maps, particle analysis, and thin film analysis, supporting applications in process technology, manufacturing/quality control, environmental hazards assessment, material fabrication, characterization of occurrence and distribution of chemical components in materials. Typical applications include metallurgical and anthropological studies; failure, thin films, particulate, mineral, and ceramic analysis; and, art history, among many others [54, 55].

4.2.6 Atomic Force Microscopy (AFM)

Atomic Force Microscopy is a technique used to image surfaces and individual protein molecules or small aggregates of such molecules on flat surfaces with high spatial resolution [51, 56, 57], being able to operate in liquids [57]. It gives use of a flexible cantilever, on which a tip is mounted due to van der Walls interactions [50]. A laser focus on the tip and its deflection is measured as the cantilever suffers electrostatic repulsion and attraction between an atom at the tip and an atom on the surface, through atomic-scale measurements of cantilever arm movements. AFM instruments have two methods of imaging, contact mode and tapping mode. In contact mode, the tip is in permanent contact with the surface, used mostly for rigid specimens once the tip can damage the soft specimens. In tapping mode, the tip oscillates at a frequency near the resonant frequency of the cantilever. The interaction of tip and surface influences the amplitude of oscillation and the oscillating frequency of the tip [50]. This microscopy is useful to measure how variations in surface characteristics, such as topography, chemistry, and electrical/electrochemical state, affect protein-surface interactions. AFM is a tool that can be used to understand the surface-protein interactions [56]. It may process the topographic images also in 3D. Their uses include several areas: Biology, Chemistry, Materials Chemistry, etc., and can be applied to many types of samples. This equipment also provides other complementary information, such as: roughness, adhesion force, and elasticity.

4.2.7 Zeta Potential (ZP)

Zeta potential relates to the nature and the charge of the samples and also with the properties of the electrolyte solution, being influenced by the pH and by the electrolyte concentration. This technique is based on the fact that one of the major surface effects is electrokinetic's. Each colloid carries an electric charge which produces a force of mutual electrostatic repulsion between adjacent particles. If the charge is high enough, the colloids will remain disperse and in suspension; if the opposite occurs, and the charge is reduced or eliminated, the colloids will steadily agglomerate and settle out of the suspension or form an interconnected matrix. Referring this phenomenon to a surface, it is intuitive to understand that the interface between a solid, a surface, and a surrounding electrolyte solution also shows a charge distribution different from both phases. The excess of one ion species and the depletion of the other ion species lead to the formation of an electrochemical double layer. This double layer is composed by an immobile layer and a diffuse layer. In the first one there is an arrangement with ions and counterions. The different number of charges creates an electrical potential between the interface and the bulk phases. The application of an external force parallel to the solid/liquid interface leads to a relative motion between the solid and liquid phases. The position of the shear plane between the immobile and diffuse layers is determined by the equilibrium between the attractive surface forces and the external forces. The electrokinetics or zeta potential is therefore an indicator of the structure and mechanism of formation of the electrochemical double layer. Modifications of the liquid phase change the structure of the electric double layer, reflected by the degree of dissociation and the variation in zeta potential. These variations are strongly dependent on the pH of the aqueous solution. Consequently the software gives other parameters namely viscosity, dielectric constants, temperature, and pH. There are several cell types depending on the samples features: the cylindrical cell for fibbers and granules; the powder cell, for powders or granules bigger than 25μm; the rectangular cell for flat samples that can be easily cut; and the clamping cell for rigid and flat samples [58].

4.3 Protein studies

To evaluate protein adsorption onto the films some techniques were employed. One of these techniques was AFM, which is described in the previous section.

4.3.1 Radiolabelling

The most widely used technique for measuring protein adsorption to surfaces uses radiolabelled proteins. It is a very sensitive and reliable technique to obtain quantitative information about proteins adsorbed to surfaces but offers no information about proteins conformation and it generates hazard waste [51]. The radiolabelling technique uses radioactive ions (like ^{125}I) and binds them to the protein of interest. After the labelling, the desired studies are performed, and the protein adsorbed is quantified by a simple measurement in the γ-counter (which counts the radioactivity of the samples). A technique useful to overcome the drawbacks of the radiolabelling is the atomic force microscopy which offers a view of individual protein molecules or small collections of such molecules adsorbed to surfaces [51].

4.3.2 Fluorescence Spectroscopy

Fluorescence spectroscopy is a technique in which the molecules of the sample to analyze have a low energy state of interest, and an excited electronic state of higher energy. Each of these electronic states has various vibrational states. In this technique the species are first excited, by absorbing a photon, from its ground electronic state to one of the various vibrational states in the excited electronic state. Collisions with other molecules cause the excited molecule to lose vibrational energy until it reaches the lowest vibrational state of the excited electronic state. The molecule then drops down to one of the various vibrational levels of the ground electronic state again, emitting a photon in the process. As molecules may drop down into any of the vibrational levels of this ground state, the photons will have different energies, and thus different frequencies. Therefore, by analysing the different frequencies of light emitted in fluorescent spectroscopy, the structure of these different vibrational levels can be

determined. Among instrumental techniques, fluorescence spectroscopy is recognized as one of the more sensitive method [59].

Molecules in solution are usually excited by UV light and the excitation source is usually a deuterium or xenon lamp. Broad-band excitation light from a lamp passes through a monochromator, which passes only a selected wavelength. The fluorescence is dispersed by another monochromator and detected by a photomultiplier tube. The excitation monochromator scanning gives the excitation spectrum and the fluorescence monochromator scanning gives the fluorescence spectrum. Simple instruments sometimes use only a bandpass filter to select the excitation wavelength [60].

There is a wide range of applications for fluorescence in this field. Large biological molecules can have a fluorescent chemical group attached by a chemical reaction, and the fluorescence of the attached tag enables very sensitive detection of the molecule. Analytical applications include quantitative measurements of molecules in solution and fluorescence detection in liquid chromatography [60].

5. References

[1] Gogolewski, S. Nonmetallic Materials for Bone Substitutes. European Cells and Materials Vol 1 Suppl. 2 (2001): 54-55;

[2] Temenoff, JS, Mikos, AG. Injectable biodegradable materials for orthopaedic tissue engineering. Biomaterials 21 (2000): 2405-2412;

[3] Gisep, A. Research on ceramic bone substitutes: current status. Injury, Int. J. Care Injured 33 (2002): S-B-88–92;

[4] Ribeiro, CC, Barrias, CC, Barbosa, MA. Calcium phosphate alginate microspheres as enzyme delivery matrices. Biomaterials 25 (2004): 4363-4373;

[5] Bonfield W. Biomaterials Research and development. In: European White Book on Fundamental Research in Materials Science, Max-Planck Institut Fur Metallforschung Stuttgart (2001);

[6] Laurencin CT, Lu HH. Polymer-ceramic composites for bone tissue engineering. In: Davies JE, editor. Bone engineering. EM Squared Inc (2000), Toronto, Canada;

[7] Schnettler R, Stahl JP, Alt V, Pavlidis T, Dingeldein E. Calcium phosphate-based bone substitutes. Eur J Trauma 4 (2004): 219-229;

[8] Sims CD, Butler PEM, Casanova R, Lee BT, Randolf MA, Lee WPA, Vacant CA, Yamremchuk MJ. Injectable cartilage using polyethylene oxide polymer substrates; Kulseng B, Skjak-Braek G, Ryan L, Anderson A, King A, Faxvaag A, Espevik T. Transplantation of alginate microcapsules. Transplantation 67 (1999): 843-850;

[9] Grifith LG, Naughton, G. Tissue engineering: current challenges and expanding opportunities. Science 295 (2002): 1009-1014;

[10] Hench LL, Polak, JM. Third-generation biomedical materials. Science 295 (2002): 1014-1017;

[11] Temenoff, JS, Mikos, AG. Injectable biodegradable materials for orthopaedic tissue engineering. Biomaterials 21 (2000): 2405-2412;

[12] Grimandi, G, Weiss, P, Millot, F, Daculsi, G. In vitro evaluation of a new injectable calcium phosphate material. J Biomed Mater Res 39 (1998): 660-666;

[13] Gisep, A. Research on ceramic bone substitutes: current status. Injury, Int. J. Care Injured 33 (2002): S-B-88–92;

[14] Ribeiro, CC, Barrias, CC, Barbosa, MA. A novel route for the preparation of injectable ceramic porous microspheres for bone tissue engineering. Ravaglio: 228-232;
[15] Gogolewski, S. Nonmetallic Materials for Bone Substitutes. European Cells and Materials Vol 1 Suppl. 2 (2001): 54-55;
[16] Ooms, EM, Wolke, JGC, van der Waerden, JPCM, Jansen, JA. Trabecular bone response to injectable calcium phosphate (Ca-P) cement. J Biomed Mater Res 61 (2002): 9-18;
[17] Fellah, BH, Weiss, P, Gauthier, O, Rouillon, T, Daculsi, G, Layrolle, P. Bone Repair Using a New Injectable Self-Crosslinkable Bone Substitute. J Orthop Research 24 (2006): 628-635;
[18] Trojani, C, Boukhechba, F, Scimeca, JC, Vandenbos, F, Michiels, JF, Daculsi, G, Boileau, P, Weiss, P, Carle, GF, Rochet, N. Ectopic bone formation using an injectable biphasic calcium phosphate/Si-HPMC hydrogel composite loaded with undifferentiated bone marrow stromal cells. Biomaterials 27 (2006): 3256–3264;
[19] Vandiver J, Deanb D, Patel N, Bonfield W, Ortiz C. Nanoscale variation in surface charge of synthetic hydroxyapatite detected by chemically and spatially specific high-resolution force spectroscopy. Biomaterials 26 (2005): 271-283;
[20] Aoki, H. Medical Applications of Hydroxyapatite. Ishiyaku EuroAmerica, Inc. (1994), Tokyo;
[21] Rodriguez-Lorenzo LM, Vallet-Regi M, Ferreira JM. Colloidal processing of hydroxyapatite. Biomaterials 22 (2001): 1847-1852;
[22] Regi, MV, González-Calbet, JM. Calcium phosphates as substitution of bone tissues. Progress in Solid State Chemistry 32 (2004): 1-31;
[23] Popescu ML, Piticescu RM, Petrescu Ş, Zdrenţu L, Mihăilescu I, Socol G, Lojkowski W. Biocompatibility of hydroxyl-apatite thin films obtained by pulsed laser deposition. Rev Adv Mater Sci 2 (2004): 164-169;
[24] Lee, KY, Peters, MC, Anderson, KW, Mooney, DJ. Controlled growth factor release from synthetic extracellular matrices. Nature 408 (2000): 21-28;
[25] www.azonano.com/details.asp?ArticleID=1538;
[26] Grifith LG, Naughton, G. Tissue engineering: current challenges and expanding opportunities. Science 295 (2002):1009-1014;
[27] Ribeiro CC, Barrias CC, Barbosa MA. A novel route for the preparation of injectable ceramic porous microspheres for bone tissue engineering. Proceedings of the

8th Meeting and Seminar on: Ceramics, Cells and Tissues. March 19-21 (2003), Faenza, Italy;

[28] Barrias CC, Ribeiro CC, Martins MC, Barbosa MA, Rodriguez D, Sá Miranda C. Calcium Phosphate Microspheres for Localised Delivery of a Therapeutic Enzyme. Key Engineering Materials 2006

[29] Barrias CC, Ribeiro CC, Barbosa MA. Adhesion and proliferation of human osteoblastic cells seeded on injectable hydroxyapatite microspheres. Key Engineering Materials 254-256 (2004): 877-880;

[30] Barrias CC, Ribeiro CC, Lamghari MM, Sá Miranda C, Barbosa MA. Proliferation, activity and osteogenic differentiation of bone marrow stromal cells cultured on calcium titanium phosphate microsphere. J Biomed Mater Res 72A (2005): 57-66;

[31] Barrias CC, Ribeiro CC, Rodriguez D, Sá Miranda C, Barbosa MA. Effect of Calcium Phosphate Addition to Alginate Microspheres: Modulation of Enzyme Release Kinetics and Improvement of Cell Adhesion. Key Engineering Materials 284-286 (2005): 689-692;

[32] van der Wal, E, Oldenburg, SJ, Heij, T, Denier van der Gon, AW, Brongersma, HH, Wolke, JGC, Jansen, JA, Vredenberg, AM. Adsorption and desorption of Ca and PO4 species from SBFs on RF-sputtered calcium phosphate thin film. Applied Surface Science 252 (2006): 3843-3854;

[33] Feddes, B, Vredenberg, AM, Wolke, JGC, Jansen, JA. Bulk composition of r.f. magnetron sputter deposited calcium phosphate coatings on different substrates (polyethylene, polytetrafluoroethylene, silicon). Surface and coating Technology 185 (2004): 346-355;

[34] van Dijk K, Schaeken HG, Marée CHM, Verhoeven J, Wolke JCG, Habraken FHPM, Jansen JA. Influence of Ar pressure on r.f. magnetron-sputtered $Ca_5(PO_4)OH$ layers. Surface and Coatings Technology: 76-77 (1995): 206-210;

[35] Strayer. *Biochemistry* (4^{th} Ed). W.H. Freeman and Company (1998), New York;

[36] http://www.chemie.fu-berlin.de/chemistry/bio/amino-acids_en.html;

[37] http://www.bio.davidson.edu/Courses/Molbio/aatable.html;

[38] http://library.thinkquest.org/C004535/amino_acids.html;

[39] Cavaleiro, A, Vieira, MT. *Textos de apoio às disciplinas de Engenharia de Superfícies e Degradação e Protecção de Superfícies* (1995). Coimbra;

[40] van Dijk, K, Schaeken HG, Wolke JCG, Jansen JA.. Influence of annealing temperature on RF magnetron sputtered calcium phosphate coatings. Biomaterials 17 (1996): 405-410;

[41] Xu, S, Long, J, Sim, L, Diong, CH, Ostrikov, KK. RF Plasma Sputtering Deposition of Hydroxyapatite Bioceramics: Synthesis, Performance, and Biocompatibility Plasma Process Polym 2 (2005): 373–390;

[42] Ozeki, K, Yuhta, T, Fukui, Y, Aoki, H. Phase composition of sputtered films from a hydroxyapatite target. Surface and Coatings Technology 160 (2002): 54-61;

[43] Ozeki, K, Aoki, H, Fukui. Effect of pH on crystallization of sputtered hydroxyapatite film under hydrothermal conditions at low temperature. Journal of Materials Science 40 (2005): 2837-2842;

[44] Thian, ES, Huang, J, Best, SM, Barber, ZH, Bonfield, W. Magnetron co-sputtered silicon-containing hydroxyapatite thin films – an in vito study. Biomaterials 26 (2005): 2947–2956;

[45] Yang, Y, Kim, KH, Ong, JL. A review on calcium phosphate coatings produced using a sputtering process – an alternative to plasma spraying. Biomaterials 26 (2005): 327-337;

[46] Wolke, JCG, De Groot, K, Jansen, JA. In vivo dissolution behaviour of various RF magnetron-sputtered Ca-P coatings on roughened titanium implants. Biomaterilas 24 (2003): 2623-2629;

[47] Wolke, JGC, De Groot, K, Jansen, JA. Dissolution and adhesion behaviour of radio-frequency magnetron-sputtered Ca-P coatings. Journal of Materials Science 33 (1998): 3371-3373;

[48] Nelea, V, Morosanu, C, Iliescu, M, Mihailescu, IN. Microestructure and mechaninal properties of hydroxyapatite thin films grown by RF magnetron sputtering. Surface and Coatings Technology 173 (2003): 315-322;

[49] Vickerman, JC. *Surface analysis – The principal Techniques*. John Wily & Sons Inc. (1999), Chichester;

[50] Ratner, BD, Hoffman, AS, Schoen, FJ, Lemons, JE. *Biomaterials Science – An Introduction to Materials in Medicine* – 2nd Edition. Elsevier Academic Press (2004), London;

[51] Chittur, KK. FTIR/ATR for protein adsorption to biomaterial surfaces. Biomaterials 19 (1998): 357-369;

[52] Andrade, JD, Smith, LM, Gregonis, DE. *Surface and Interfacial Aspects of Biomedical Polymers, Vol 1, Surface chemistry and Physics*. Plenum Press (1985), New York;

[53] Brás, M. Difracção de Raios-X (1999). Aveiro;

[54] http://www.emc.sc.edu/Instrumentation/cameca/sx50/index.html;

[55] http://epmalab.uoregon.edu/;

[56] Gettens, RTT, Bai Z, Gilbert, JL. Quantification of the kinetics and thermodynamics of protein adsorption using atomic force microscopy. J Biomed Mater Res 72 A (2005): 246-257;

[57] Wadu-Mesthrige, K, Amro, NA, Liu, GY. Immobilization of Proteins on Self-Assembled Monolayers. Scanning Vol. 22 (6) (2000): 380-388;

[58] Zeta-Meter Inc. Manual;

[59] http://en.wikipedia.org/wiki/Fluorescence_spectroscopy;

[60] http://www.chemistry.adelaide.edu.au/external/soc-rel/content/mol-fluo.htm.

1. Material and Methods

1.1 Preparation of the sputtered films

Thin films of HA, Ti, and HA doped with different titanium concentrations ranging from 8 to 26% (at%) were sputtered on gold substrates using an RF magnetron equipment (Edward Coating System E306A) and argon as the sputtered gas.

Gold substrates were produced by deposition of chromium (5 nm) and gold (25 nm) films onto silicon wafers. The layer of chromium was used to improve adhesion of gold to silicon. The wafers were coated with 1.5 mm of photoresist, to protect the film surface. The removal of the photoresist was performed by ultrasonic washing with water (4 min), acetone (3 min), and water (2 min).

For the deposition of the ceramic films, two different targets were used: a hydroxyapatite commercial sintered disk (purity 99.99%) and 1 cm^2 titanium plates (purity 99.3%). The substrate had no Bias and the operation power of the target was between 250 W (for Ti films) and 450 W (for the doped films except for HATi16, which was 300 W due to plasma instability). The deposition pressure was of 7.0×10^{-3} mbar. HA, Ti, and HA doped with Ti with a Ti content of 8, 16, 19, and 26 at % films, were prepared. The differences in atomic percentages were accomplished by using different number of Ti plates.

For characterization purposes, the films used in EPMA and XRD techniques were let to sputter one hour on steel substrates and their thickness ranged from 300 to 1000 nm.

Films of HA, HA doped with 8 and 16% of Ti, and Ti, with a thickness of approximately 75 nm (time of deposition 5 to 10 minutes) were prepared for the biological studies, except for HA, which was let to deposit for 1 hour with a resulting thickness of 300 nm approximately.

1.2 Characterization of the sputtered films

The films were characterized using different techniques namely electron probe microanalysis (EPMA), X-ray diffraction (XRD), X-ray photoelectron spectroscopy (XPS), Fourier transformed infrared – infrared reflection absorption spectroscopy (FTIR-IRAS), contact angle measurements, atomic force microscopy (AFM), and zeta potential (ZP).

1.2.1 Electron Probe Microanalysis (EPMA)

The chemical composition of the films deposited on steel substrates was determined by electron probe microanalysis (EPMA) using a Cameca SX 50 equipment.

1.2.2 X-Ray Diffraction (XRD)

The films deposited on steel substrates were analysed by glancing incident X-ray Diffraction using a Philips X'PERT diffractometer PW 1710 apparatus with Co Kα radiation, in a θ-2θ Bragg-Brentano mode. Since sputtered films are amorphous, a thermal treatment at 600ºC for 5 hours in controlled atmosphere was performed in an attempt to increase their crystallinity.

1.2.3 X-Ray Photoelectron Spectroscopy (XPS)

XPS measurements were carried out on a VG Scientific Escalab 200A (UK) spectrometer using magnesium Kα (1253.6 eV) as a radiation source. The photoelectrons were analyzed with a take off angle of 55º. Survey spectra were collected over a range of 0-1150 eV with analyzer pass energy of 50 eV. High-resolution spectra of C 1s, O 1s, P 2p, Ca 2p and Ti 2p, were collected with analyzer pass energy of 20 eV. All the spectra were curve fitted using asymmetrical Gaussian-Lorentzian profiles.

1.2.4 Fourier Transform Infrared – Infrared Reflection Absorption Spectroscopy (FTIR – IRAS)

FTIR spectra were obtained using a Perkin Elmer 2000 FT-IR spectrometer with an IRAS accessory. An MCT (mercurium, cadmium, tellurium) detector was used and five hundred scans were accumulated in order to obtain a high signal-to-noise level. Spectra were collected over a range of 700-4000 cm^{-1}. A nitrogen purge of the sample compartment was performed to minimize artefacts that could arise from residual air bands (CO_2 and H_2O vapour).

1.2.5 Contact Angle Measurement

In order to evaluate the surface energy of the films, contact angle of water droplets onto the surfaces were measured using a Data Physics GA 15 system, equipped with a video CCD-camera and SCA 20 software. The films were placed in a closed, thermostated chamber at 25 ºC saturated with water in order to prevent evaporation from the drop. Sessile drop method was used to calculate the contact angle between 4 μl water drops and the samples, using droplet profiles fitting through mathematical functions, which vary depending on the contact angle. Young-Laplace fitting method was used to calculate contact angles higher or equal to 90º and the ellipse fitting method for contact angles comprised between 90º and 30º. The contact angle of each surface was then calculated by extrapolating the time dependent curve to zero.

1.2.6 Atomic Force Microscopy (AFM)

Surface morphology and roughness of the films were evaluated using an atomic force microscope from molecular imaging (Pico Scan Controler). For each sample, different randomly chosen areas were analyzed. The instrument was operated in tapping mode in air with a 10×10 μm^2 piezo scanner. A silicon nitride tip with a spring constant of 42 N/m was used. The average roughness (Sa), the standard deviation of the amplitude (Sq), the maximum peak (Smax), and the surface area (S3A) were determined using scanned areas of 5×5 μm.

1.2.7 Zeta Potential (ZP)

Zeta potential measurements were performed in an Electro Kinetic Analyzer, from Anton Paar at physiological pH (7.4) using a KCl (1mM) solution as electrolyte. A clamping cell, appropriated for flat and rigid samples was used. Measurements were made based on the Fairbrother-Mastin's method.

2. Results and Discussion

2.1 Electron Probe Microanalysis (EPMA)

Films with atomic titanium percentages ranging from 0 to 26% were obtained as shown in Table 1.

The microprobe analysis of the as-deposited thin films also showed that the Ca/P ratio of the HA films was higher than 1.67 indicating the presence of a secondary calcium phase. This phase could possibly be calcium oxide, which is normally present in calcium phosphate sputtered films [1-4]. It was also observed that the Ca/P ratio increased with the Ti percentage (except for the Ti-26% films), suggesting that there is a competition between Ti and P in the deposition process and/or P is being sputtered out from the growing film by other incoming atoms, possibly due to the weak phosphorous binding energy [4-6].

Table 1. EPMA atomic percentages and elemental ratios for the as-deposited films.

Substrates	Atomic %				Ratios	
	O	P	Ca	Ti	Ca/P	(Ca+Ti)/P
HA	67,26	11,43	21,31	0,00	1,86	0,00
HATi-0,2%	71,72	11,22	16,87	0,19	1,50	1,86
HATi-8%	65,27	8,30	18,79	7,65	2,26	1,52
HATi-16%	65,55	4,01	14,82	15,62	3,70	3,19
HATi-19%	64,25	3,19	13,40	19,16	4,20	7,59
HATi-26%	56,82	5,60	11,63	25,94	2,08	10,21

2.2 X-Ray Difraction (XRD)

X-ray diffraction analysis (Figure 1) showed that all the thin films were amorphous as it was expected since the lack of crystallinity is a common charateristic of ceramic sputtered systems [1, 2, 4-9]. However, after heat treatment (Figure 2), only HA films crystallinity was increased, indicating that the presence of Ti destabilizes the HA lattice, thus inhibiting its crystallization.

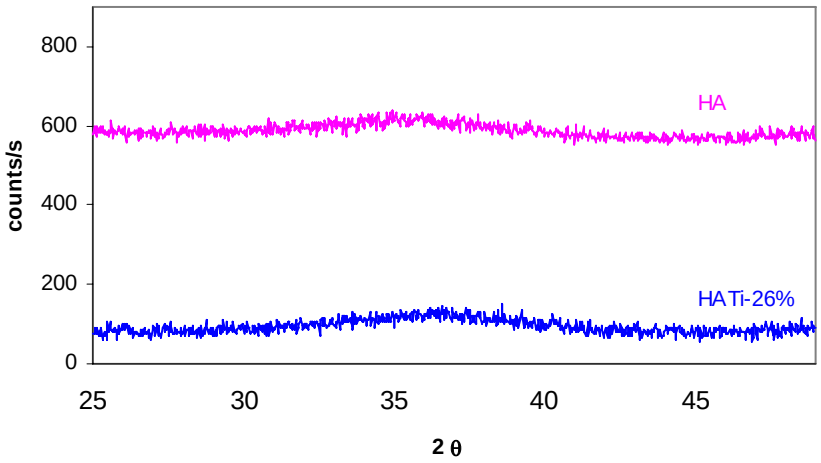

Figure 1. XRD spectra of HA and HATi26 as deposited films.

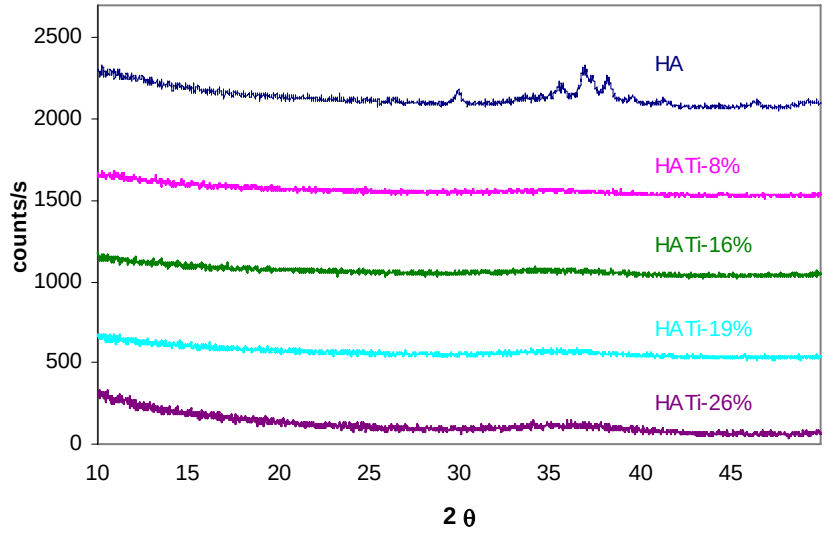

Figure 2. XRD spectra of HA and HATi films after heat treatment.

The more intense peaks characteristic of HA are not present in the XRD diffractogram of the heat treated HA sample indicating that the structure of the thin film formed is preferentially orientated as a consequence of the deposition technique [10].

2.3 Fourier Transform Infrared – Infrared Reflectance Absorption Spectroscopy (FTIR – IRAS)

Figure 3 shows the FTIR spectra of HA and HA doped with Ti as deposited films on steel substrates. It can be observed that an increase in the Ti percentage of the films resulted in the broadening of the characteristic phosphate bands (1154 and 1014 cm^{-1}) suggesting a decrease in crystallinity. For each film composition, similar spectra were obtained before and after heat treatment (Figure 4). In what concerns the 75 nm thick films deposited on gold substrates, the FTIR spectra of the as deposited films present some differences when compared to the ones deposited on steel (Figure 5). This is possibly due to the different times of deposition used and consequently in the thickness and organization of the films.

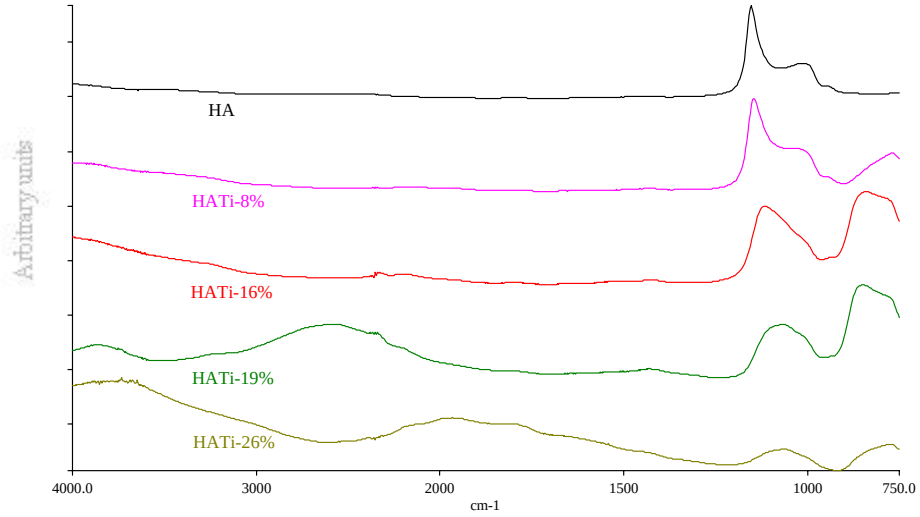

Figure 3. FTIR spectra of HA and HATi as deposited films.

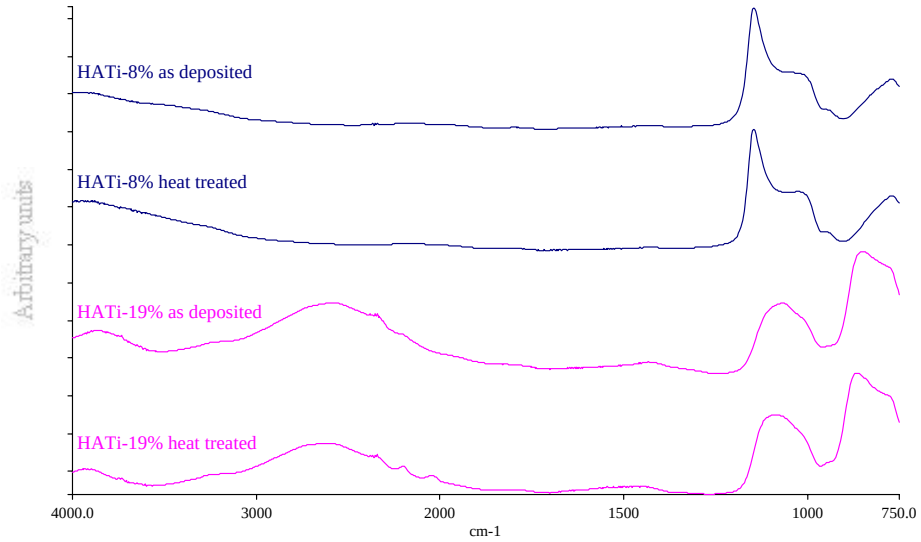

Figure 4. FTIR spectra of HATi8 and HATi16 films before and after the heat treatment, at 600º for 5 h in controlled atmosphere.

The FTIR spectrum of HA films 75 nm thick (Figure 5) is characterized by two bands in the ν_3 (PO_4^{3-}) region (900–1200 cm^{-1}) namely at 1108 and 947 cm^{-1}. The broad bands at 3271 cm^{-1} and 1602 cm^{-1} can be attributed to the lattice water. In general lattice water absorbs in the region 3200–3550 cm^{-1} (antisymmetric ν_3 and ν_1 modes and symmetric OH stretching) and at 1600-1650 cm^{-1} (HOH bending ν_2 mode) [11]. Similarly to what was observed in the thicker films, the insertion of Ti causes the broadning of the phosphate bands indicating a decrease in the crystallinity. It is also observed characteristic bands of the carbonate group, namely the ones corresponding to the the ν_3 vibration of C-O between 1410 and 1470 cm^{-1} and the the ν_2 vibrations between 850 and 880 cm^{-1}.

The band at 3642 cm^{-1} is assigned to O-H vibrations suggesting the presence of an hydroxide compound. As previously mentioned, calcium oxide is normally present as secondary phase in calcium-phosphate sputtered films. Calcium oxide is an unstable phase that rapidly reacts when in contact with moisture leading to the formation of calcium hydroxide.

In order to eliminate this secondary phase, the substrates were washed in de-ionized water. Different immersion times were used, namely 10, 60, and 240 minutes. It was observed that for an immersion period of 10 minutes the 3642 cm^{-1} band dissapeared. For a time of immersion of 240 minutes there is a significant decrease in the FTIR absorption peak heights (Figure 6, Figure 7, and Figure 8), indicating that the films were

partially dissolved. This is due to the fact that sputtered films are poorly crystalline and consequently unstable in water solution.

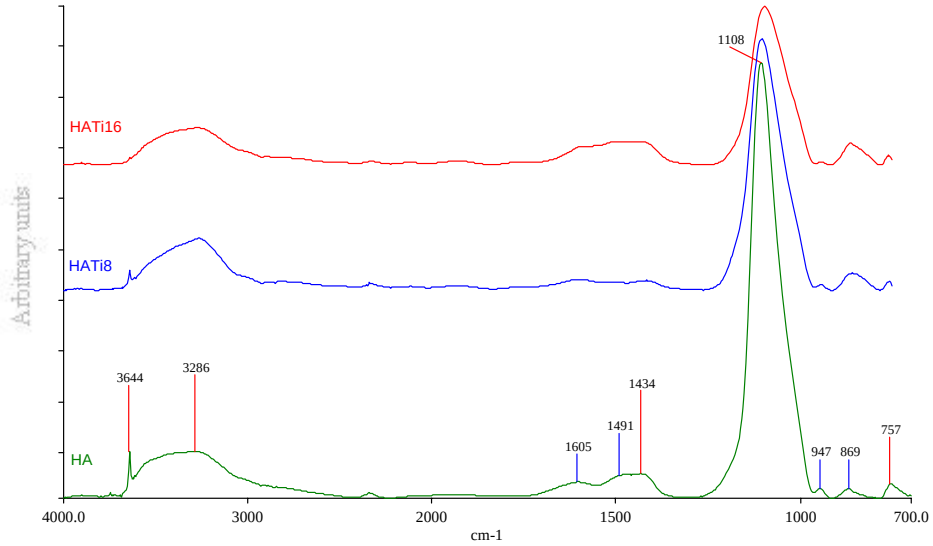

Figure 5. FTIR spectra of HA and HA doped with Ti films as deposited.

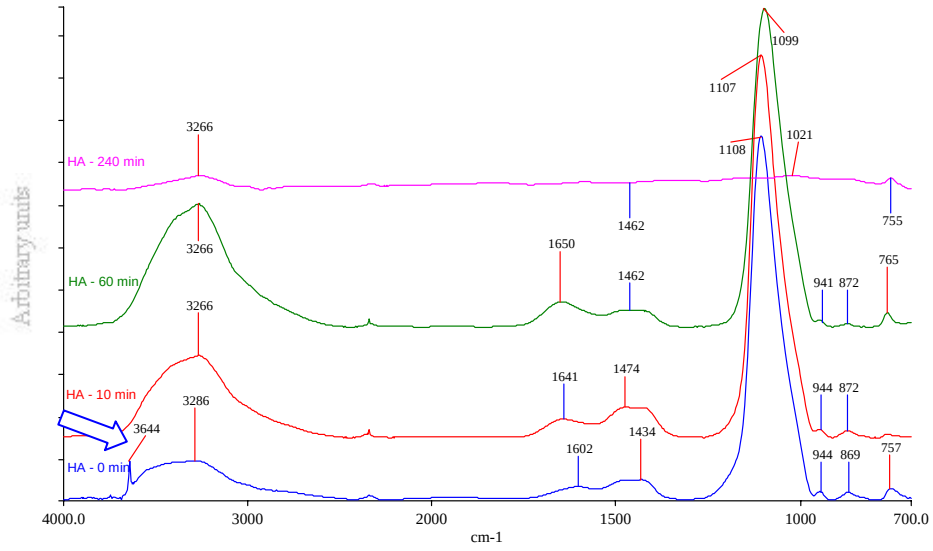

Figure 6. FTIR spectra of HA films as deposited and after immersion in de-ionized water for different times (10, 60, and 240 minutes).

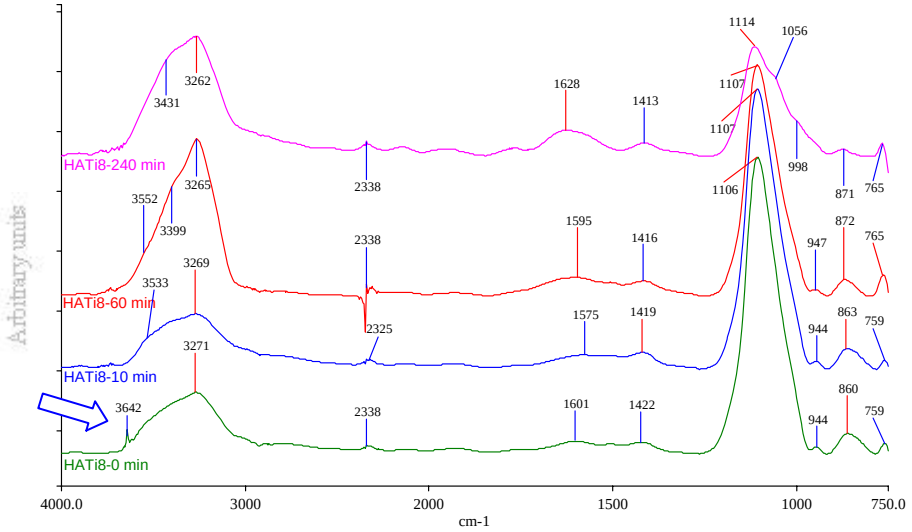

Figure 7. FTIR spectra of HATi8 films as deposited and after immersion in de-ionized water for different times (10, 60, and 240 minutes).

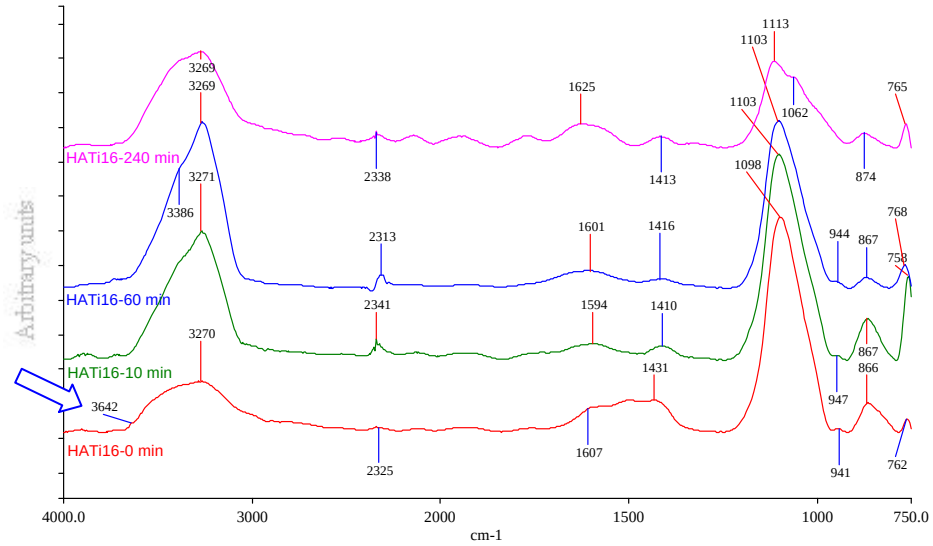

Figure 8. FTIR spectra of HATi16 films as deposited and after immersion in de-ionized water for different times (10, 60, and 240 minutes).

2.4 X-Ray Photoelectron Spectroscopy (XPS)

XPS core levels of the P2p, Ca2p, Ti2p, and O1s orbital were examined for each film. XPS analysis of the different substrates showed a shift in the binding energy of Ca and P bands as the percentage of Ti in the films increased (Figure 9 to Figure 12), suggesting that structural changes are occuring as consequence of the insertion of Ti in the films.

The fact that high resolution O1s spectra delineated non symmetrical peak for all the films indicates that more than one oxigen specie is present on each surface, supporting the presence of CaO in the films.

For a titanium concentration of 26%, XPS results suggest the formation of a new Ti-P rich phase, since the deconvolution of P2p spectra resulted in a duplet (Figure 11) not assigned to PO_4 groups.

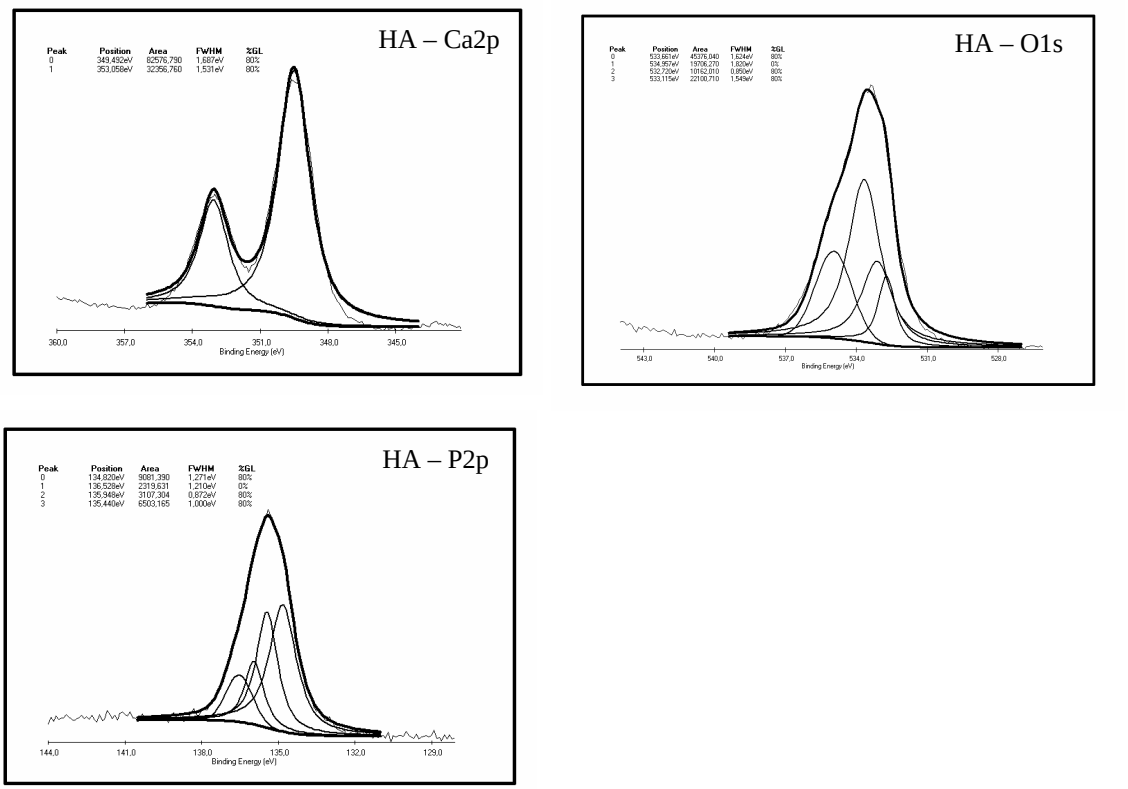

Figure 9. Ca2p, O1s, P2p, and Ti2p high resolution spectra for the HA as deposited thin films.

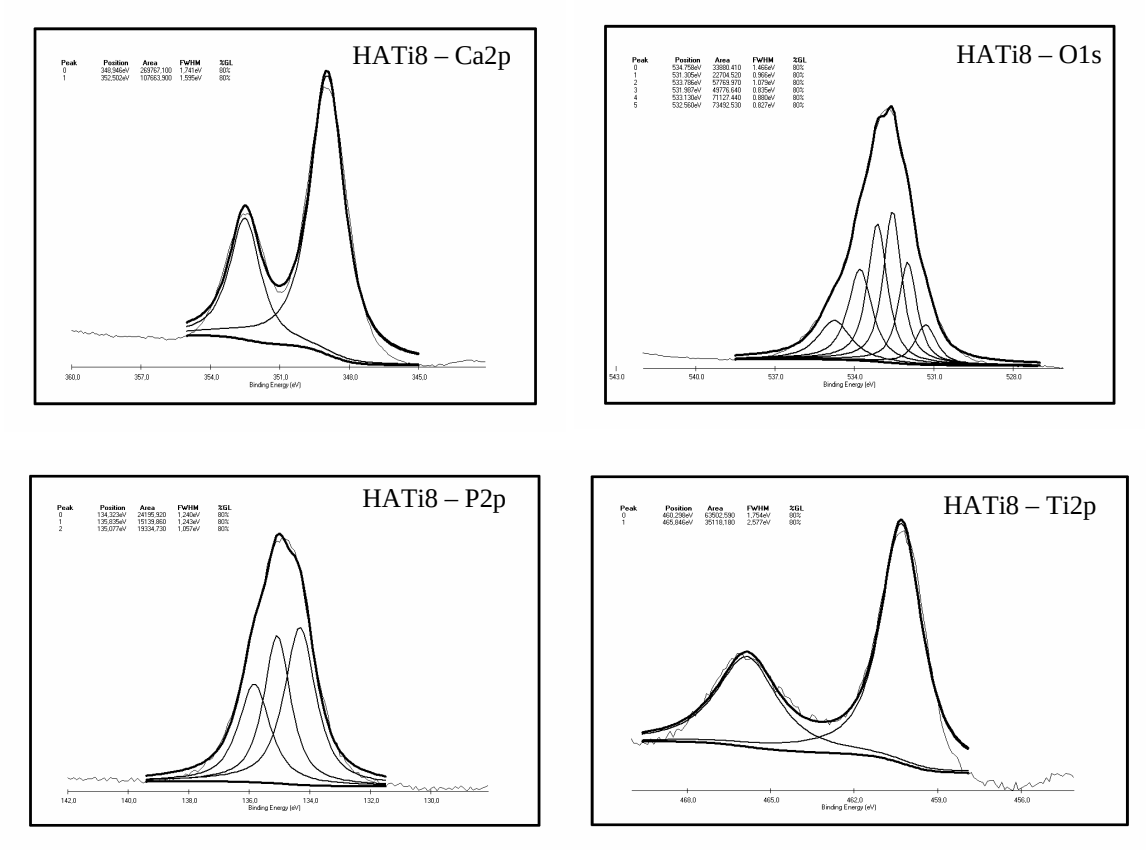

Figure 10. Ca 2p, O 1s, P 2p, and Ti 2p high resolution spectra for the HATi8 as deposited thin films.

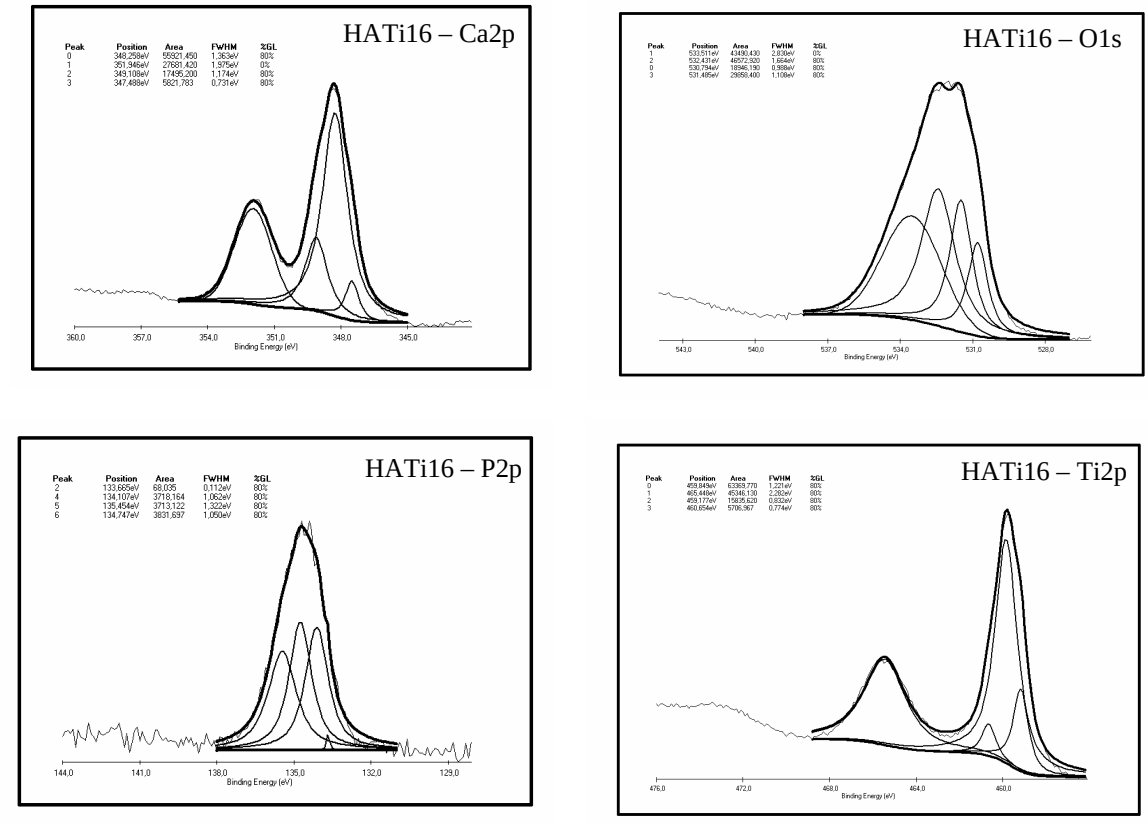

Figure 11. Ca2p, O1s, P2p, and Ti2p high resolution spectra for the HATi16 as deposited thin films.

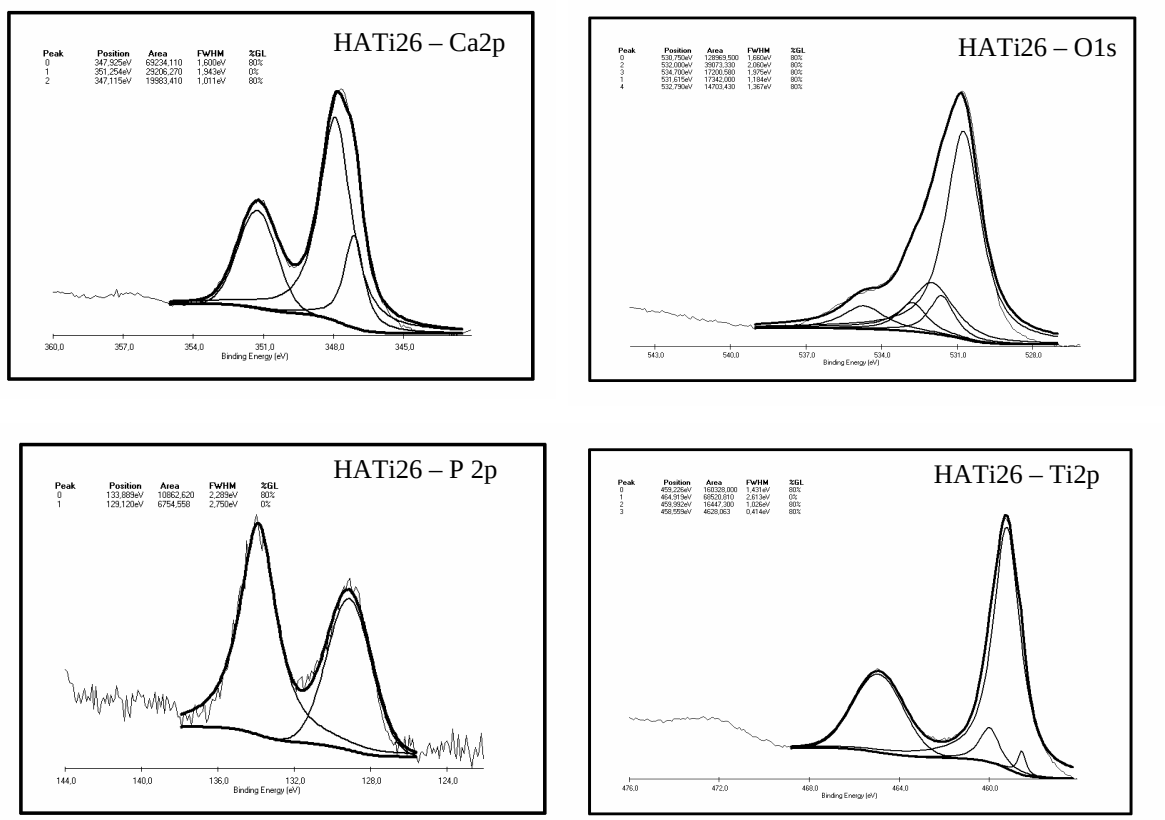

Figure 12. Ca2p, O1s, P2p, and Ti2p high resolution spectra for the HATi26 as deposited thin films.

2.5 Contact Angle Measurement

In order to evaluate if the presence of Ti changed the wetting properties of the substrates wettability studies were performed. It was shown that the contact angle of the films ranged from 85 to 102º and no correlation between contact angle and Ti concentration could be established.

After the washing procedure the contact angle dropped, especially for the films doped with Ti (101º to 42º and 103 to 72º for HATi8 and HATi16, respectively). The other films also showed a decrease in the contact angle, but not so drastic, keeping their hydrophobicity (95º to 90º and 92º to 80º for HA and Ti, respectively).

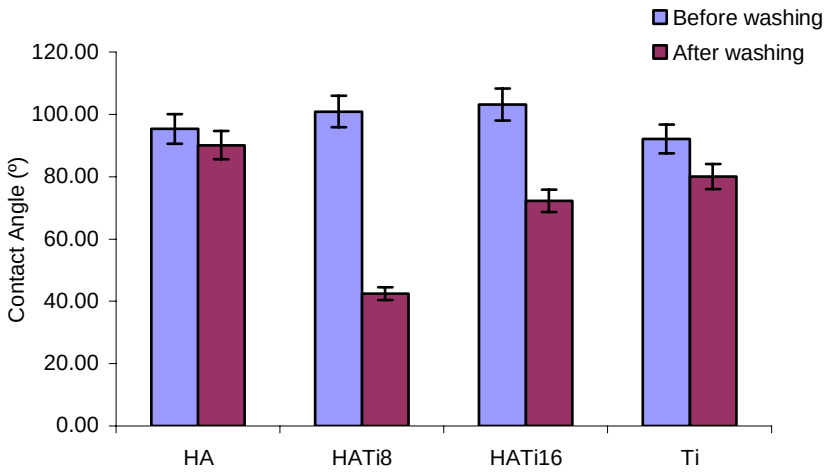

Figure 13. Contac angles between the different films and drops of water, before and after the washing procedure.

2.6 Atomic Force Microscopy (AFM)

The AFM analysis showed that the surface roughness of HA coatings was significantly higher than the roughness of the other films (results not shown). In order to overcome this discrepancy, HA films were let to sputter for one hour (instead of 7 minutes). The topographic images of the different films in 2D and 3D are presented in Figure 14 and Figure 15. The different surfaces exhibited characteristic morphology and surface roughness (Table 2).

The 5 μm scan of each coating shows that small features are present in all the samples varying in size and distribution (Figure 14 and Figure 15).

In what concerns HA films, the surface has uniformly distributted round features with a diameter ranging from 100 to 300 nm, and a maximum depth in height of approximately 60 nm. The surface morphology of the two titanium doped films is very similar as well as their average surface roughness. A high density of features of 150 to 350 nm can be observed on their surfaces forming, in some cases, agglomerates.

The Ti films are considerably smoother than the other films, having surface features of approximately 100 nm.

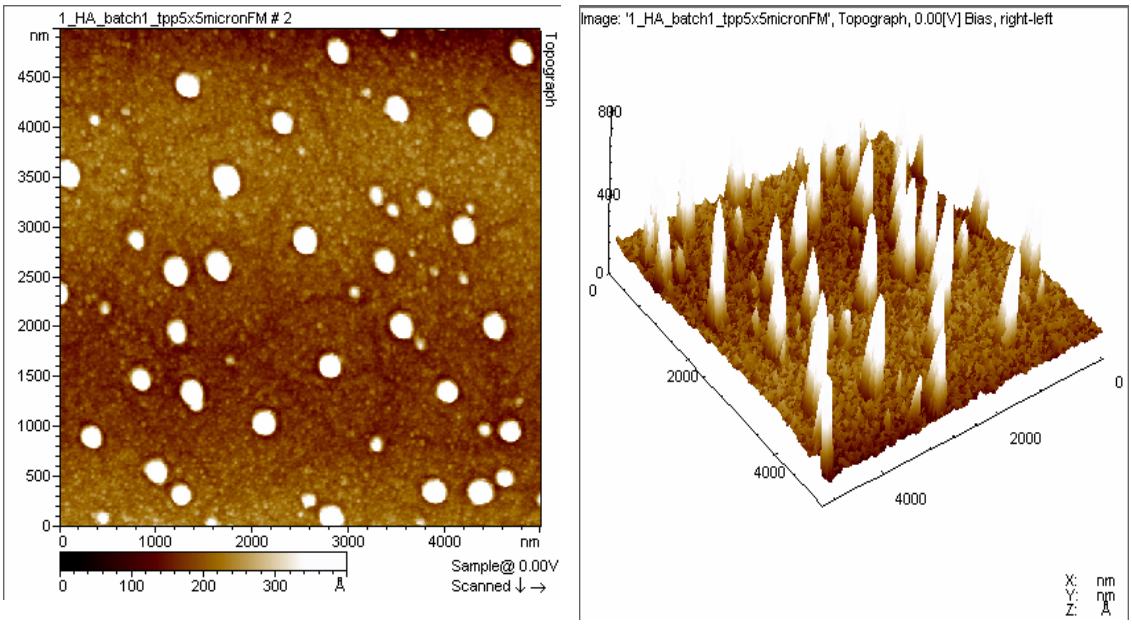

HA

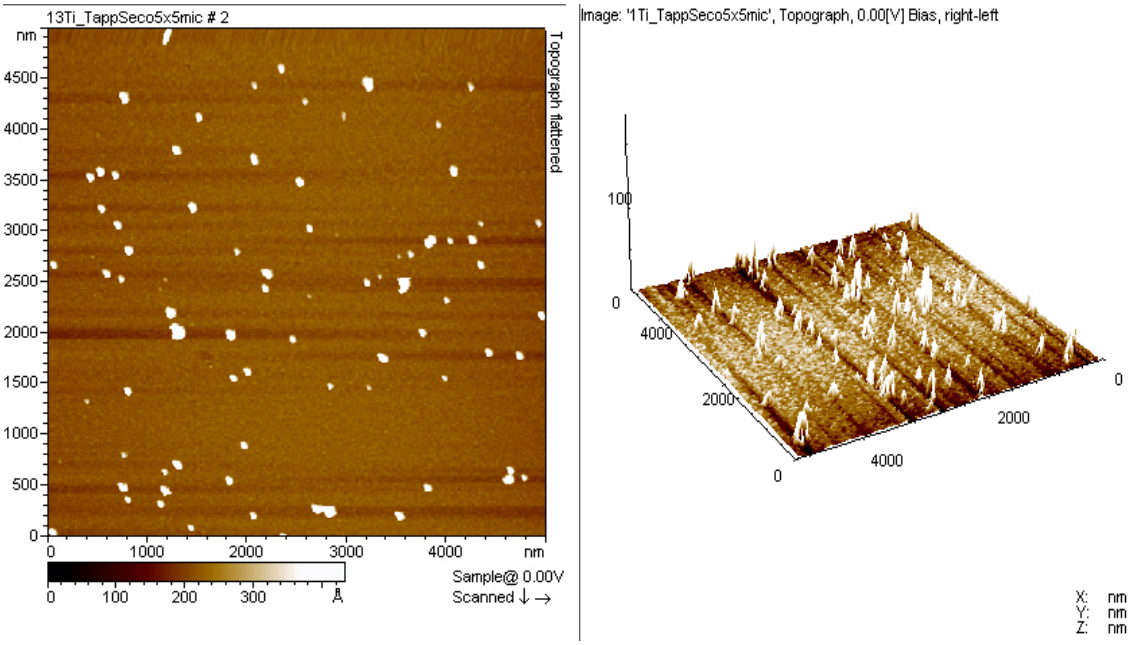

Ti

Figure 14. Surface profile morphology of the HA and Ti as sputtered films.

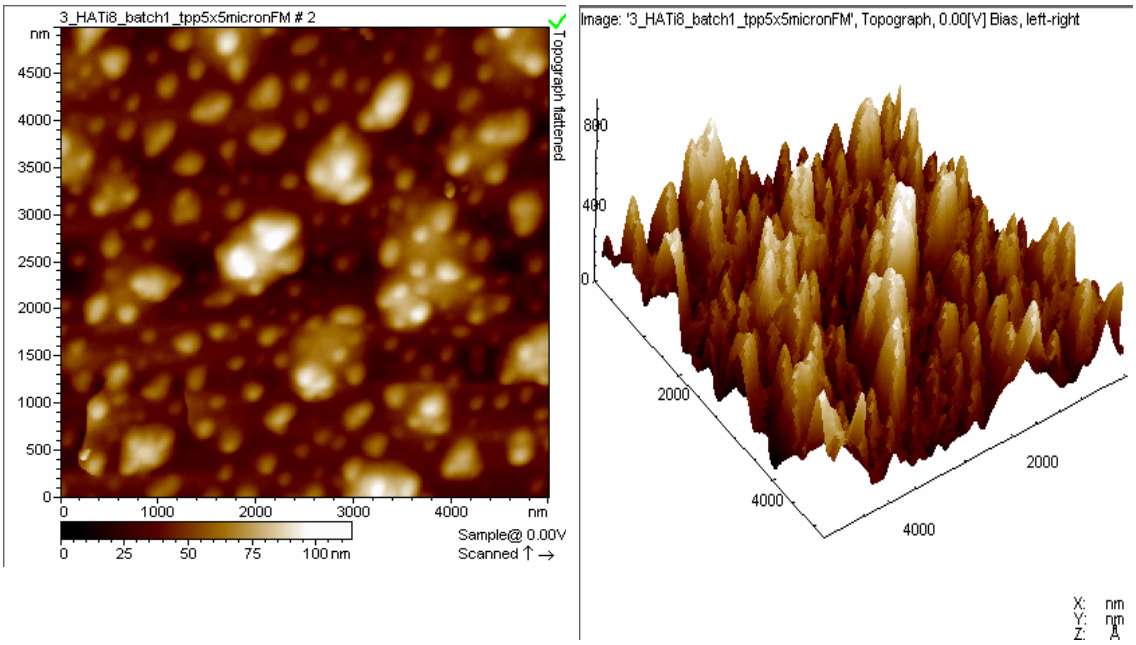

HATi8

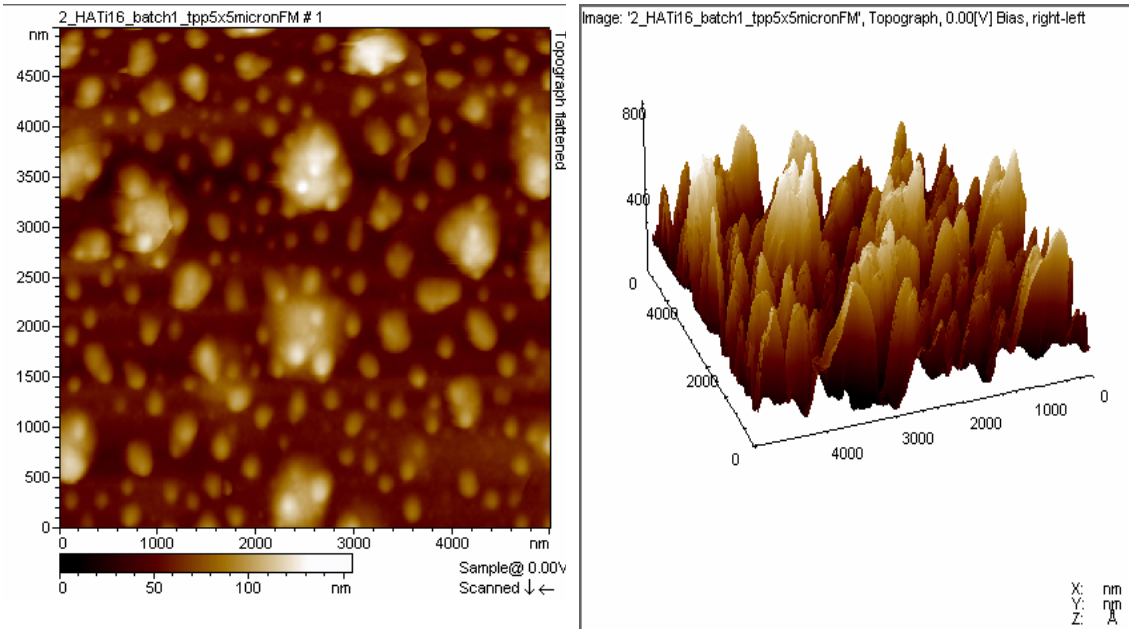

HATi16

Figure 15. Surface profile morphology of the HATi8 and HATi16 as sputtered films.

Table 2. Roughness values (Sa) and surface area (S3A), for the HA and HA doped with Ti films, given by SPIP software based on the AFM images.

		0 min	**10 min**	**60 min**	**240 min**
HA	Sa (nm)	3.61 ± 0.17	1.83 ± 0.82	0.96 ± 0.29	0.98 ± 0.05
	S3A (nm^2)	2,56E+07 ± 1.15E+05	2,53E+07 ± 1.73E+05	2,51E+07 ± 0.00E+00	2,52E+07 ± 0.00E+00
HATi8	Sa (nm)	11,90 ± 0.82	8,37 ± 0.62	8,89 ± 0.53	1,17 ± 0.00
	S3A (nm^2)	2,95E+07 ± 5.77E+04	2,52E+07 ± 5.00E+04	2,55E+07 ± 3.14E+05	2,50E+07 ± 0.00E+00
HATi16	Sa (nm)	14,03 ± 0.49	13,00 ± 0.82	11,93 ± 0.40	3,22 ± 0.12
	S3A (nm^2)	2,58E+07 ± 1.15E+05	2,61E+07 ± 2.89E+05	2,60E+07 ± 3.00E+05	2,51E+07 ± 0.00E+00
Ti	Sa (nm)	1,83 ± 1.38			
	S3A (nm^2)	2,63E+07 ± 2.00E+05			

AFM was also used to follow the changes in the films morphology during the washing procedure, in order to select the more appropriated washing time. In Figure 16 one can see the evolution of topography with increasing washing time. This study was only performed with the HA and the HA doped films, once in Ti films CaO phase is not formed. It is observed that the HA films morphology changes significantly with the increase of the washing time. After 10 minutes of immersion in water, the number and size of the round features decreases significantly. Also the surface roughness decreases with the time of immersion presenting a roughness value of 0.98 nm very alike to the gold substrate (0.50 nm) indicating that the ceramic film is practically dissolved. These results are in accordance with the ones obtained by FTIR (Figure 6). Regarding the HA doped with Ti films they seem to be more stable towards dissolution than HA. Their morphology is very similar even after a washing time of 60minutes for HATi8 sample and 240 minutes for HATi16 sample, although the number of agglomerates is reduced.

The roughness of the HA doped films slightly decreases with the increasing of the washing time until 60 minutes. For a time of immersion of 240 minutes a drastic decrease on the surface roughness is observed for both compositions.

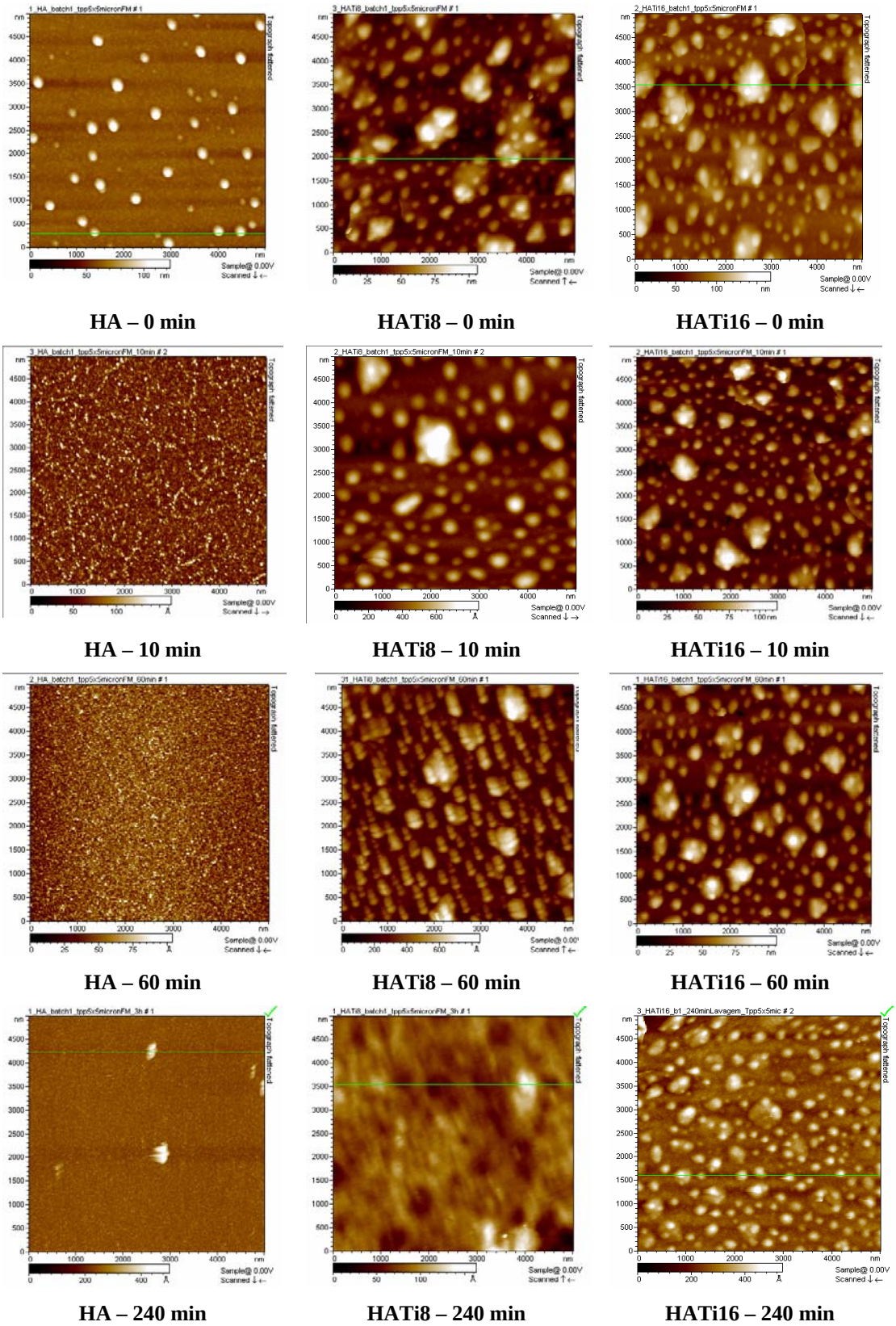

HA – 0 min | **HATi8 – 0 min** | **HATi16 – 0 min**

HA – 10 min | **HATi8 – 10 min** | **HATi16 – 10 min**

HA – 60 min | **HATi8 – 60 min** | **HATi16 – 60 min**

HA – 240 min | **HATi8 – 240 min** | **HATi16 – 240 min**

Figure 16. AFM topography images, through the different washing times, for the HA and HA doped with Ti films.

Changes in the roughness as a consequence of the washing procedure can also be observed by analysing a horizontal cross section of the topographic images (Figure 17). Peak heights change, approximately, from 65, 50, and 100 nm to 20, 10, and 25 nm, for HA, HATi8, and HATi16, respectively.

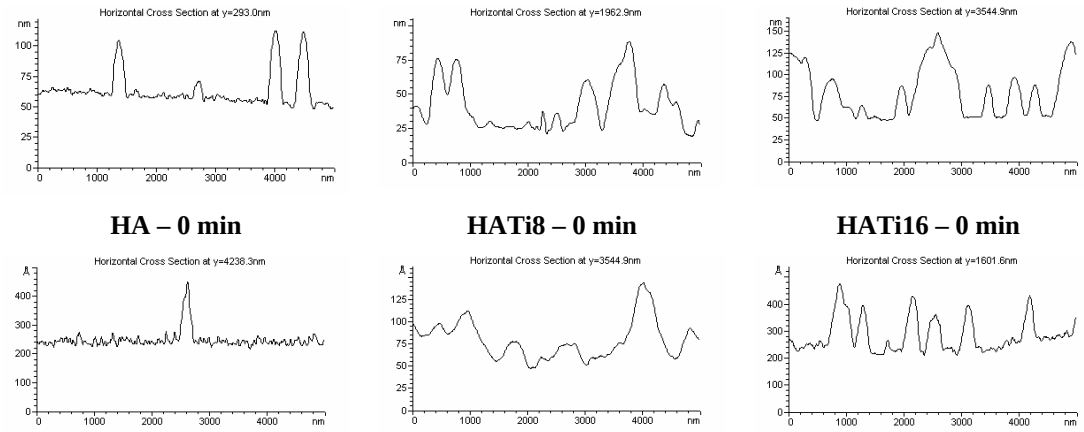

Figure 17. Horizontal cross section of the morphological images of the HA and HATi films before and after 240 minutes washing.

2.7 Zeta Potential (ZP)

Table 3 shows the zeta potential of the different surfaces. It is observed that the doped films present a more negative potential, than HA and Ti films, being the HA films the ones with a less negative zeta potential. The negative values at pH 7.4, are in agreement with those reported by other authors concerning potential measurements of powder suspensions [12, 13, 14].

Table 3. Zeta potential of the different sputtered films and the correspondent standard error.

Films	Zeta potential (mV)
HA	-12.8 ± 1.71
HATi8	-20.82 ± 0.21
HATi16	-21.12 ± 0.90
Ti	-15.05 ± 0.97

3. Conclusions

Using the sputtering technique it was possible to obtain amorphous HA films doped with different Ti atomic percentages. When submitted to heat treatment the doped films remain amorphous suggesting that Ti ions disturb the HA lattice, inhibiting its crystallization. The Ca/P ratio of the doped films increased with Ti concentration (except for the HATi26 films), suggesting that there is a competition between Ti and P in the deposition process and/or that P is being sputtered from the growing film by other incoming atoms. For the HATi26 films, a Ti-P rich phase seems to be formed.

CaO was present in HA and HA doped films as a secondary phase and was eliminated or significantly reduced by washing in de-ionized water for 10 minutes. The amorphous ceramic films are not stable towards dissolution and partially dissolve when immersed in water. At physiological pH all the films composition tested (HA, HATi8, HATi16 and Ti) are negatively charged, the zeta potential of the HA doped films being the more negative.

In what concerns the morphology of the coatings, round features are present in all samples varying in size and distribution.

4. References

[1] Ozeki, K, Aoki, H, Fukui. Effect of pH on crystallization of sputtered hydroxyapatite film under hydrothermal conditions at low temperature. Journal of Materials Science 40 (2005): 2837-2842;

[2] Nelea, V, Morosanu, C, Iliescu, M, Mihailescu, IN. Microestructure and mechaninal properties of hydroxyapatite thin films grown by RF magnetron sputtering. Surface and Coatings Technology 173 (2003): 315-322;

[3] Nelea, V, Morosanu, C, Iliescu, M, Mihailescu, IN. Hydroxyapatite thin films grown by pulsed laser deposition and radio-frequency magnetron sputtering: comparative study. Applied Surface Science 228 (2004):346-356;

[4] Ong, JL, Raikar, GN, Smoot, TM. Properties of calcium phosphate coatings before and after exposure to simulated biological fluid. Biomaterials 18 (1997): 1271-1275;

[5] van Dijk K, Schaeken HG, Marée CHM, Verhoeven J, Wolke JCG, Habraken FHPM, Jansen JA. Influence of Ar pressure on r.f. magnetron-sputtered $Ca_5(PO_4)OH$ layers. Surface and Coatings Technology: 76-77 (1995): 206-210;

[6] Yang, Y, Kim, KH, Ong, JL. A review on calcium phosphate coatings produced using a sputtering process – an alternative to plasma spraying. Biomaterials 26 (2005): 327-337;

[7] van Dijk, K, Schaeken HG, Wolke JCG, Jansen JA.. Influence of annealing temperature on RF magnetron sputtered calcium phosphate coatings. Biomaterials 17 (1996): 405-410;

[8] Thian, ES, Huang, J, Best, SM, Barber, ZH, Bonfield, W. Magnetron co-sputtered silicon-containing hydroxyapatite thin films – an in vito study. Biomaterials 26 (2005): 2947–2956;

[9] Wolke, JCG, De Groot, K, Jansen, JA. In vivo dissolution behaviour of various RF magnetron-sputtered Ca-P coatings on roughened titanium implants. Biomaterials 24 (2003): 2623-2629;

[10] Bunshah, RF. Handbook of Hard Coatings – Deposition Technologies, Properties and Applications. Noyes Publications (2001) New Jersey, USA;

[11] Socrates L. Infrared and Raman Characteristic Group Frequencies – Tables and Charts. John Wiley & Sons, Ltd: (2001) Chichester, England;

[12] Ribeiro, CC, Barrias, CC, Barbosa. A novel route for the preparation of injectable ceramic porous microspheres for bone tissueengineering. Key engineering (2004): 228:232;

[13] Ferraz MP, Monteiro FJ, Serro AP, Saramago B, Gibson IR, Santos JD. Effect of chemical composition on Hydrophobicity and Zeta potential of plasma sprayed HA/CaO-P2O5 glass coatings. Biomaterials 22 (2001): 3105-3112;

[14] Lopes MA, Monteiro FJ, Santos JD, Serro AP, Saramago B. Hydrophobicity, surface tension and zeta potential measurements of glass reinforced hydroxyapatite composites. Journal of Biomedical Materials Research 45 (1999): 370-375.

1. Materials and Methods

1.1 Preparation of the substrates

Films of HA, Ti, and HA doped with Ti (8 and 16% at%) were used as model surfaces for human serum albumin (HSA) and glucocerebrosidase (GCR) adsorption studies.
The films were prepared as previously described in Chapter II (Section 1.1).

1.2 Human Serum Albumin (HSA) adsorption studies

1.2.1 Preparation of the protein solution

A 0.1 mg/mL HSA solution was prepared by dissolving HSA (Sigma, ref A1653) in degassed phosphate buffered saline (PBS) (Sigma, pH 7.4). For radiolabelling purposes HSA was dissolved in PBS with 0.01 M of NaI (iodinated PBS, PBSI). Buffer with iodine (PBSI) was used to inhibit adsorption of free radioactive iodide [1].

1.2.2 Adsorption of HSA onto the substrates

The amount of HSA adsorbed to the films was quantified using ^{125}I-HSA. HSA was labelled with ^{125}I according to the Iodogen method where iodination was performed at 0ºC in an Eppendorf tube coated with Iodogen (sigma) and evaporated with a gentle flow of nitrogen. Purification of ^{125}I-HSA to remove free iodine was performed using Sephadex G-25M columns (PD-10, Amersham Pharmacia biotech). The yield of the iodination reaction was approximately 93%, as determined by precipitating the ^{125}I-HSA with 20% trichloroacetic acid (TCA) (Merck). ^{125}I-HSA was added to unlabelled HSA solution in order to obtain a final activity of 2×10^8 cpm/mg.
For the HSA adsorption measurements, the samples were placed in a 24-well tissue culture plate (Sarstedt) with the coating facing up. A drop of PBS was added to the periphery of each well to maintain moisture and a 7 μL drop of HSA solution was pipetted onto each film. Protein adsorption was carried out at 25ºC over a 30 minutes period [2]. After rinsing the samples for four times with 2 mL of PBS, the radioactivity was counted in a γ-counter.

HSA surface concentration was calculated using the following equation:

$$\text{HSA (mg/m}^2\text{)} = [\text{Counts (cpm)} \times C_{solution}\ \text{(mg/mL)}] / [A_{solution}\ \text{(cpm/mg)} \times \text{SA (m}^2\text{)}]$$

where the Counts, are the radioactivity measurements from the films, $C_{solution}$ the concentration of the solution, $A_{solution}$ the specific activity of the solution, and SA is the surface area of the sample in contact with the drop. The drop contact area was determined using the surface area of the samples given by the SPIP AFM software and the diameter of the drop measured using the contact angle instrument facilities. Desorption tests with HSA were also performed, by immersing the substrates with adsorbed HSA in a PBS solution (25ºC) for 24 hours, after which samples were rinsed four times with 2 mL of PBS and counted for radioactivity.

1.2.3 Analysis of the substrates after HSA adsorption

1.2.3.1 Atomic Force Microscopy (AFM)

For the AFM imaging, samples were immersed in 1 mL of the HSA solution for 30 minutes at 25ºC. After that, samples were washed 4 times with 2 mL of 0.01M PBS in order to remove any non-adsorbed HSA molecules. Before and after protein adsorption, samples were immersed in 0.01M PBS and imaged in MAC mode (Magnetic Alternating Current mode), at room temperature, with the collection of both topographic and phase data.

1.2.3.2 Fourier Transform Infrared – Infrared Reflectance Absorption Spectroscopy (FTIR – IRAS)

FTIR spectra were obtained using a Perkin Elmer 2000 with an IRAS accessory FT-IR spectrometer. An MCT (mercurium, cadmium, tellurium) detector was used and five hundred scans were accumulated in order to obtain a high signal-to-noise level. Spectra were collected over a range of 700-4000 cm^{-1}. A nitrogen purge of the sample compartment was performed to minimize artefacts that could arise from residual air bands (CO_2 and H_2O vapour).

1.3 Glucocerebrosidase (GCR) adsorption studies

1.3.1 Preparation of the enzyme solution

Enzyme stock solutions (2mg/mL) were prepared by reconstituting recombinant human glucocerebrosidase lyophilised powder (GCR, Genzyme Corporation) in de-ionized water. The stock solution was diluted to 0.1 mg/mL immediately prior to use, in PBS 0.01M. As for HSA protein, GCR was dissolved in PBSI for radiolabelling adsorption.

1.3.2 Adsorption of GCR onto the substrates

The adsorption of GCR was quantified using the same methodology described before for the HSA adsorption studies (1.2.2).

1.3.3 Catalytic activity evaluation of adsorbed GCR

The catalytic activity of the adsorbed enzyme was assayed as the hydrolysis of the water-soluble substrate 4-methylumbelliferyl-β-D-glucopyranoside (4-MU-Glc, Glycosynth) [3]. The incubation mixture consisted of 5 nm 4-MU-Glc and 50-100mM citrate-phosphate buffer (pH 5.5). After an incubation period of 30 minutes at 37ºC, the reaction was stopped with 1 M glycine in 30% NaOH (pH 10.3). The product 4-methylumbelliferone (4-MU) was quantified by fluorescence spectroscopy with excitation at 366 nm and emission at 445 nm using a Cary Eclipse Fluorescence Spectrophotometer (Varian, Inc.). GCR activity is reported as nmol4-MU/mL/h. The specific activity is given by nmol4-MU/mL/h/ngGCR. The amount of adsorbed GCR was obtained from the radiolabelling experiments. Free enzyme was used as a control.

2. Results and Discussion

2.1 Human Serum Albumin (HSA) adsorption studies

2.1.1 Adsorption of HSA onto the substrates

Figure 1 shows the amount of HSA adsorbed per unit surface area for the different substrates. The doped films adsorb the lowest amount of protein (1.08 mg/m^2 and 1.07 mg/m^2 for HATi8 and HATi16, respectively), followed by HA films (1.77 mg/m^2), while the Titanium films are the ones that adsorb the highest amount (3.39 mg/m^2).

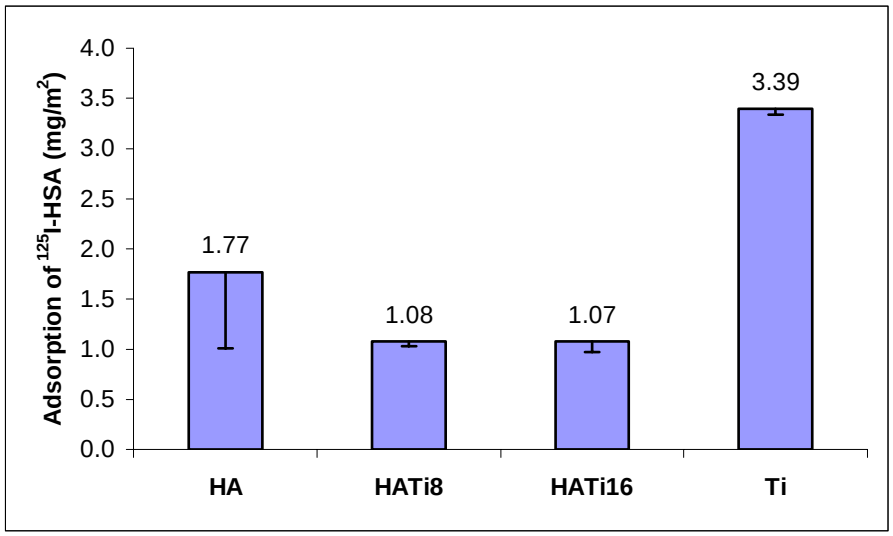

Figure 1. The amount of HSA adsorbed to the films, quantified by radiolabelling technique using ^{125}I.

The desorption studies performed with HSA, presented in Figure 2, show that the films which adsorb the highest amounts of protein (HA and Ti) are the ones that retain more protein, while the doped films (HATi8 and HATi16) retain less, though the differences are not statistically significant.

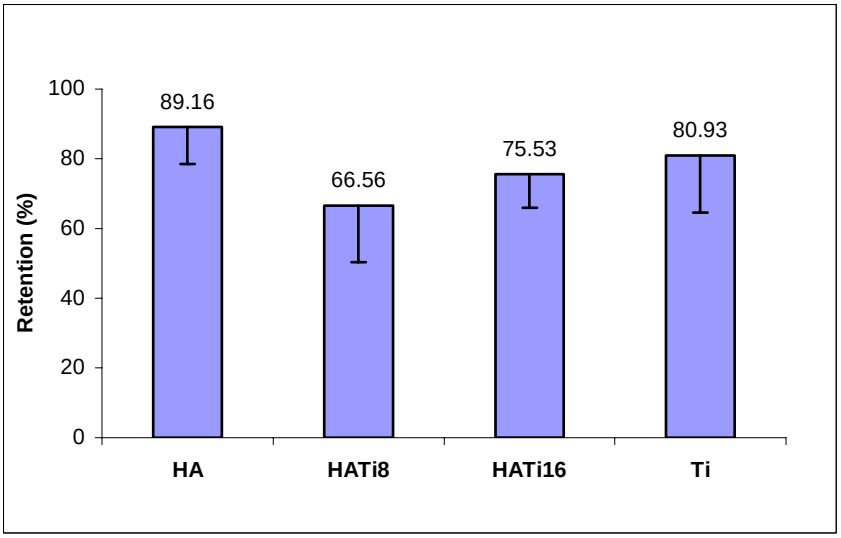

Figure 2. The percentage of retention of HSA adsorbed to the films, quantified by radiolabelling technique using ^{125}I.

2.1.2 Analysis of the substrates after HSA adsorption

2.1.2.1 Atomic Force Microscopy (AFM)

Using Atomic Force Microscopy it was possible to visualize how the protein HSA was distributed and how it affects the morphology of the different substrates (Figure 3 to Figure 6).

Since the surfaces have features that are of the same order of magnitude as protein molecules, in some cases it was difficult to distinguish protein from the substrate material. For that reason, besides topography, phase images were also obtained since they provide complementary information, particularly when samples present different surface viscoelastic properties [4].

The AFM images of the HA doped films after HSA adsorption, show an increase in the number of globular surface features. The new features can be attributed to HSA with a globular shape since they present viscoelastic characteristics that are different from the ones of the substrates prior to protein adsorption (Figures 4 and 5). In what concerns the HA and Ti films, their surface before and after protein adsorption was fairly uniform and HSA seems to adsorb as a layer and not as agglomerates (Figures 3 and 6). At physiological pH, HA doped films are more negative than HA and Ti films (Chapter II, section 2.7) and, since HSA is negatively charged, the repulsive charge will be higher for HA-doped substrates. This could partially explain the different adsorption behaviour of albumin towards the different substrates although other aspects should be taken into account namely chemical composition and surface morphology of the films.

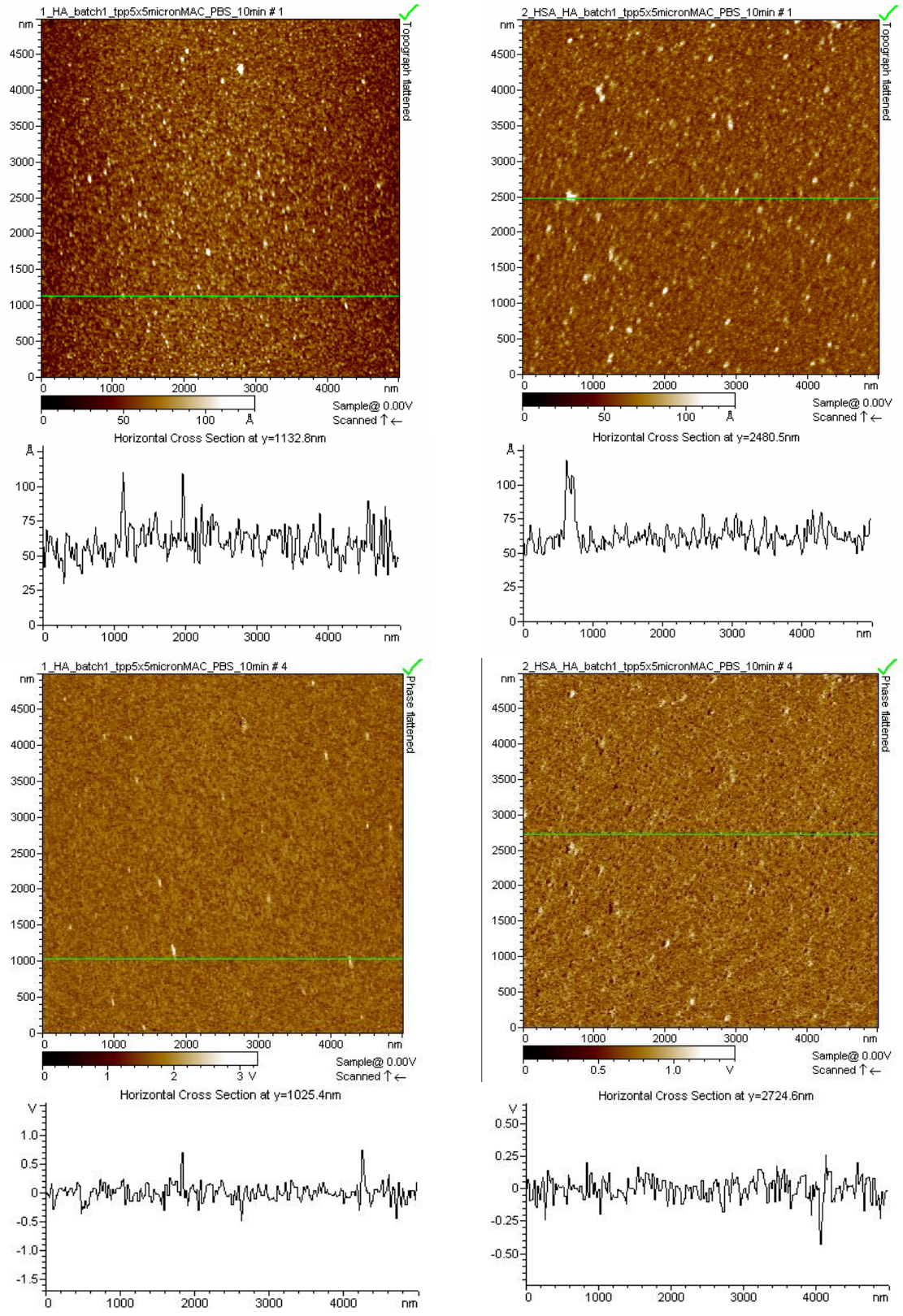

Figure 3. AFM images of the topography and phase of the HA films before and after HSA adsorption.

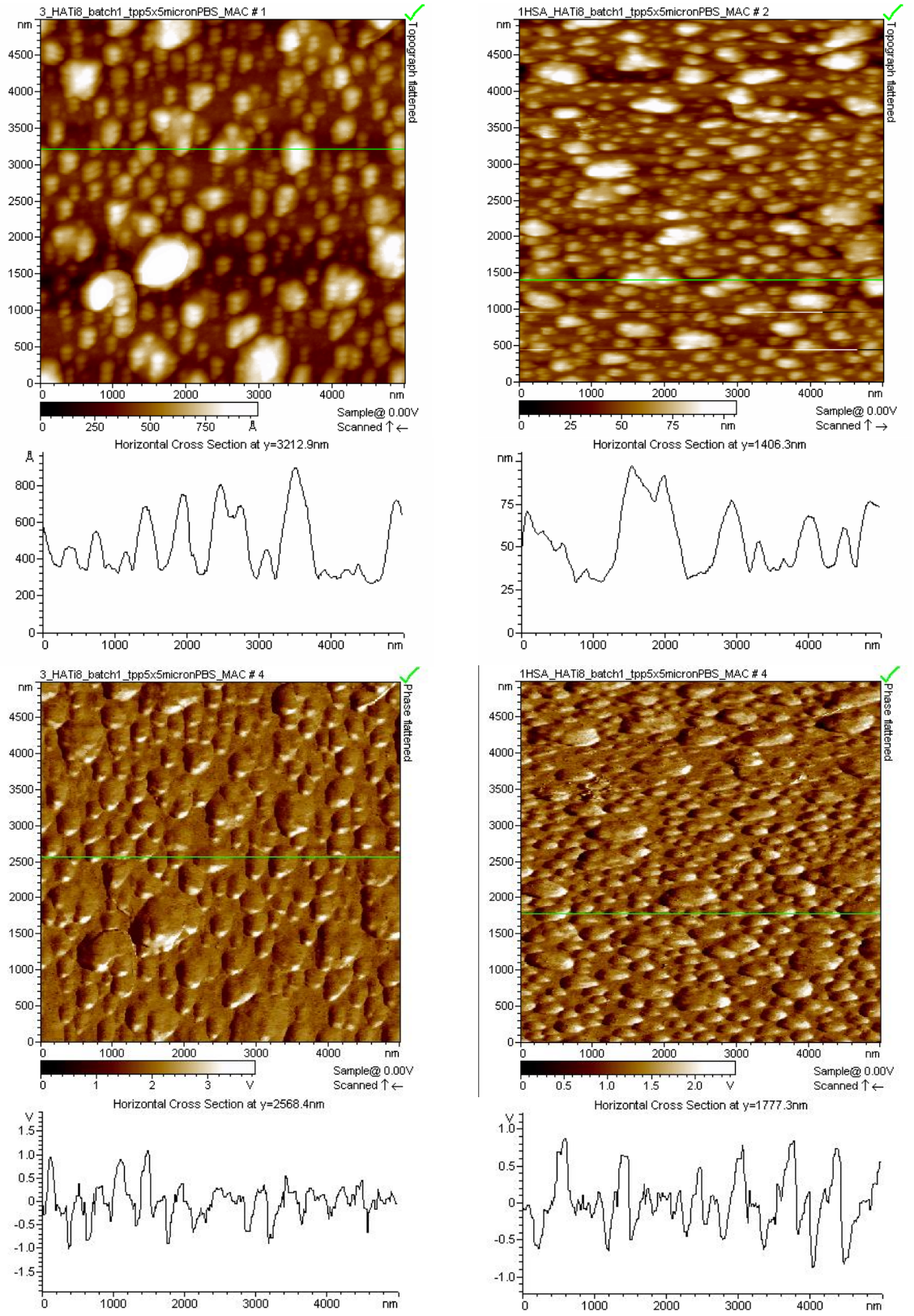

HATi8 without HSA HATi8 with HSA

Figure 4. AFM images of the topography and phase of the HATi8 films before and after HSA adsorption.

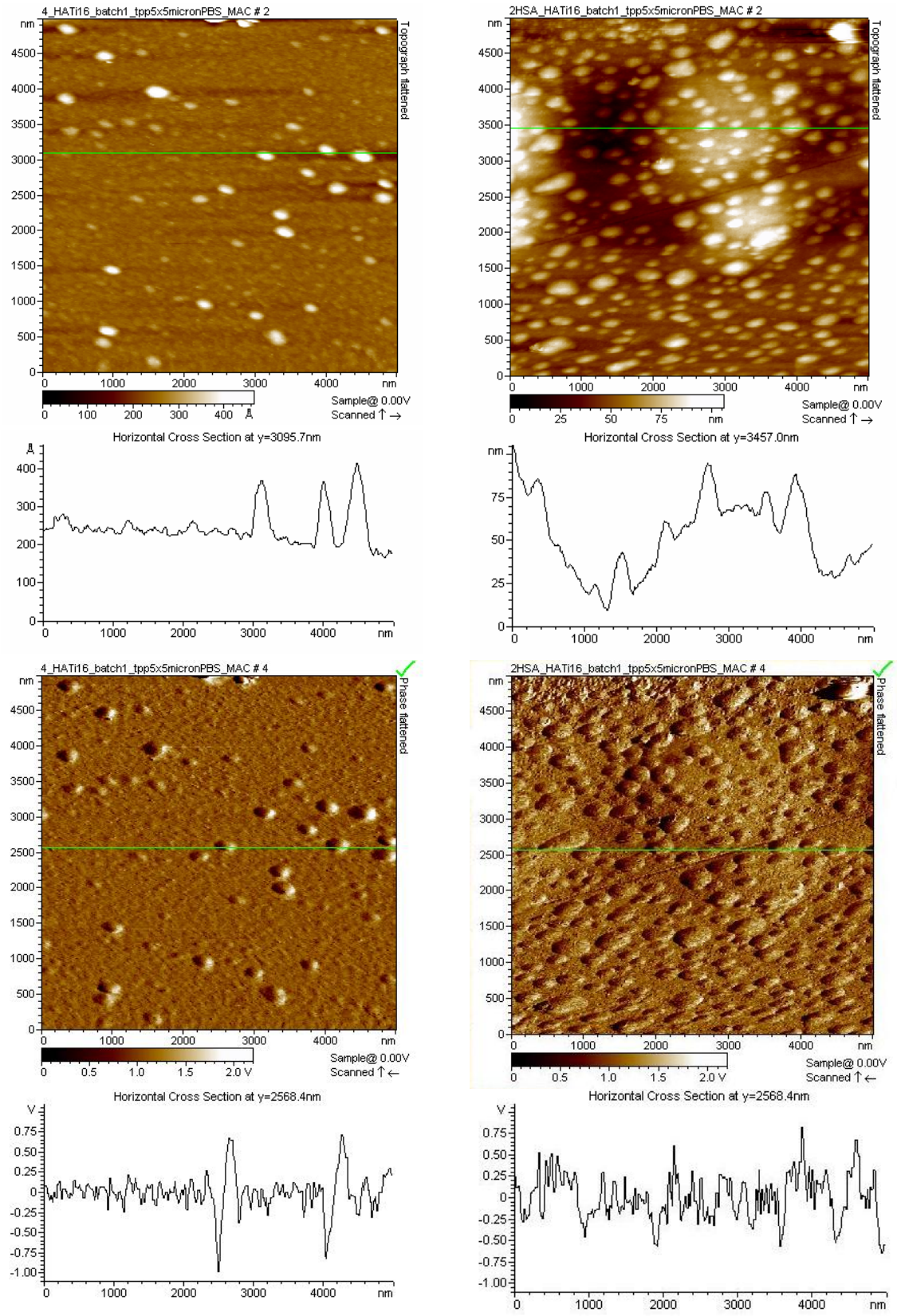

HATi16 without HSA HATi16 with HSA

Figure 5. AFM images of the topography and phase of the HATi8 films before and after HSA adsorption.

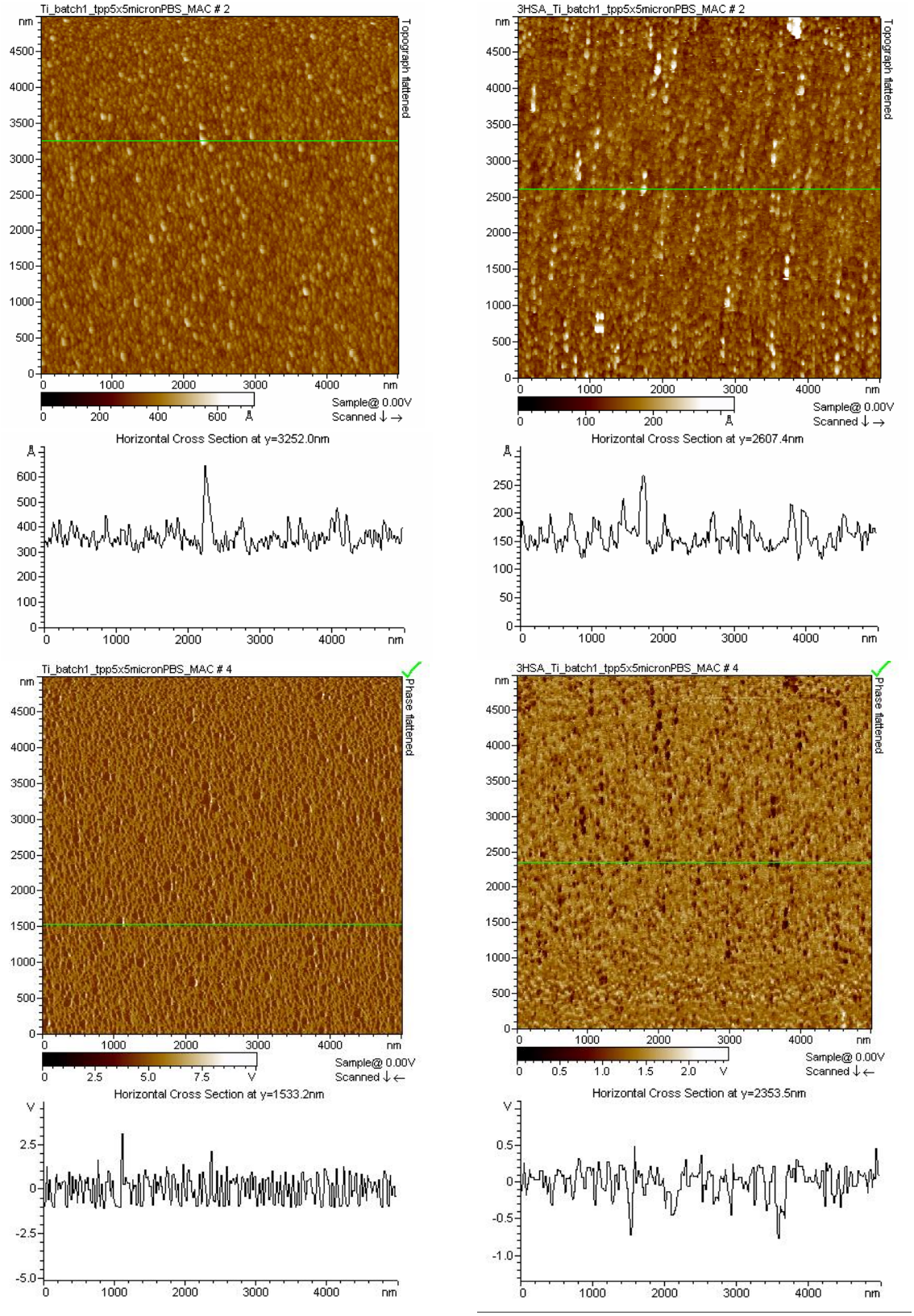

Ti without HSA Ti with HSA

Figure 6. AFM images of the topography and phase of the titanium films before and after HSA adsorption.

Table 1 shows the roughness and surface area values of the films before and after HSA adsorption. It can be observed that after protein adsorption, the roughness of HA and Ti doped films increases particularly that of HATi16 substrates, in contrast to the roughness of Ti films which decreases. The increase in surface roughness is possibly due to the fact that in those substrates HSA globules tend to adhere to the top of surface features rather than occupy valleys on the surface. Changes in surface area are in accordance with changes in roughness (Table 1).

Table 1. Roughness (Sa) and superficial area (S3A) values given by the AFM SPIP software of the films before and after the HSA adsorption.

		Without HSA	**With HSA**
HA	Sa (nm)	0,73 ± 0.05	0,84 ± 0.43
	S3A (nm^2)	2,51E+07 ± 0.00E+00	2,51E+07 ± 0.00E+00
HATi8	Sa (nm)	12,07 ± 0.21	12,50 ± 0.44
	S3A (nm^2)	2,56E+07 ± 0.00E+00	2,74E+07 ± 1.25E+06
HATi16	Sa (nm)	3,18 ± 1.35	14,80 ± 2.78
	S3A (nm^2)	2,55E+07 ± 2.08E+05	2,66E+07 ± 3.79E+05
Ti	Sa (nm)	2,96 ± 0.06	1,87 ± 0.05
	S3A (nm^2)	2,63E+07 ± 2.00E+05	2,56E+07 ± 2.65E+05

Fourier Transform Infrared – Infrared Reflectance Absorption Spectroscopy (FTIR – IRAS)

The HSA adsorption was followed by FTIR–IRAS. FTIR-IRAS spectra of the HA and HA doped films after being immersed in HSA solution show bands characteristic of Amide I (1690 ± 45 cm^{-1}) and Amide II (1540 ± 60 cm^{-1}) vibrations confirming protein adsorbed onto the substrates (Figure 7). In what concerns Ti films, FTIR-IRAS results are not conclusive since interferences arise due to the metallic substrate [5].

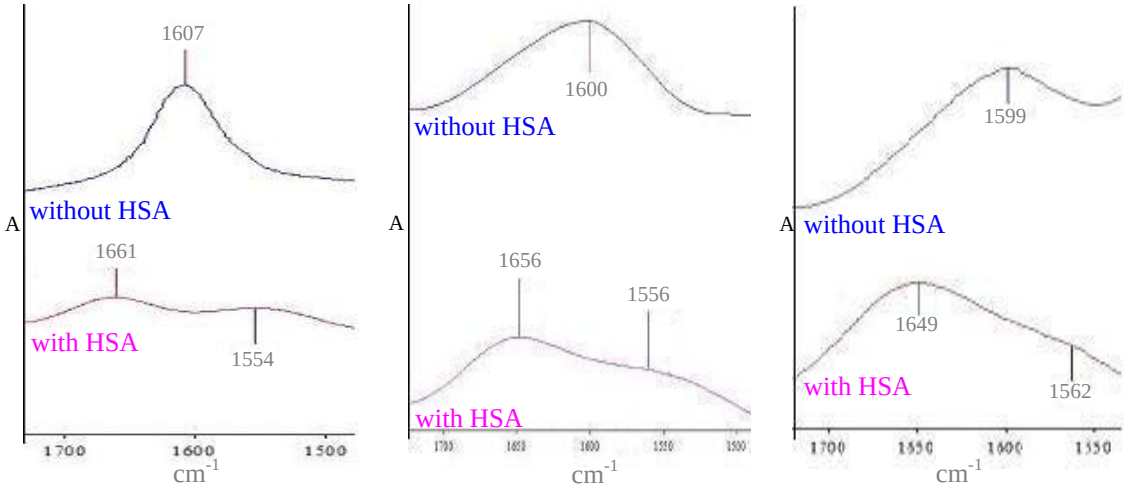

Figure 7. FTIR spectra for HA, HATi8, and HATi16 films with and without the HSA adsorbed.

2.2 Glucocerebrosidase (GCR) adsorption studies

2.2.1 Adsorption of GCR onto the substrates

Figure 8 shows the amount of GCR enzyme adsorbed to the different substrates. As it can be seen, the doped films adsorbed less amount of GCR (1.03 mg/m^2 and 0.79 mg/m^2 for HATi8 and HATi16, respectively), followed by the HA films (1.19 mg/m^2), while the Ti films adsorb more enzyme (1.88 mg/m^2). The results obtained for GCR are in accordance with the ones observed in the HSA adsorption studies, following the same pattern of adsorption.

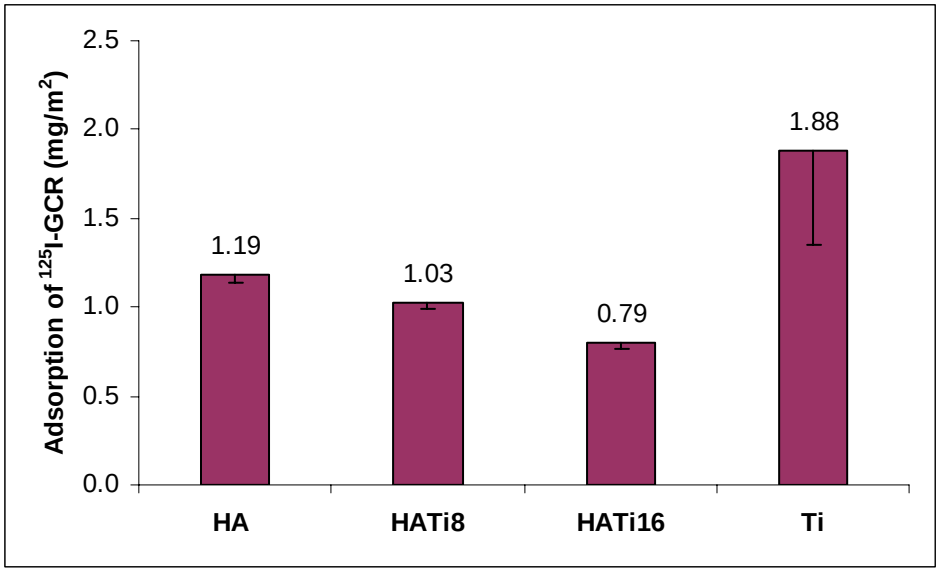

Figure 8. The amount of GCR adsorbed to the different films, quantified by radiolabelling technique using ^{125}I.

2.2.2 Catalytic activity evaluation of adsorbed GCR

The catalytic activity of the enzyme glucocerebrosidase (GCR) upon adsorption was investigated, as it may denaturate and loose its biofunctionality. This was accomplished by using a fluorescent substrate and measuring the concentration of the hydrolysis product (4-methylumbelliferone, 4-MU). The enzymatic specific activity of the adsorbed protein is expressed in nmol4-MU/mL/h/ng, and it is represented in Figure 9. The GCR activity on HA films was similar to the one of the free enzyme. As the titanium content in the films increased, the GCR activity beyond its free enzyme

activity values also increased (277, 555, and 1420 nmol4-MU/mL/h/ng for HATi8, HATi16 and Ti, respectively). The results obtained clearly show a straight connection between Ti and the enhancement of the GCR enzyme specific activity.

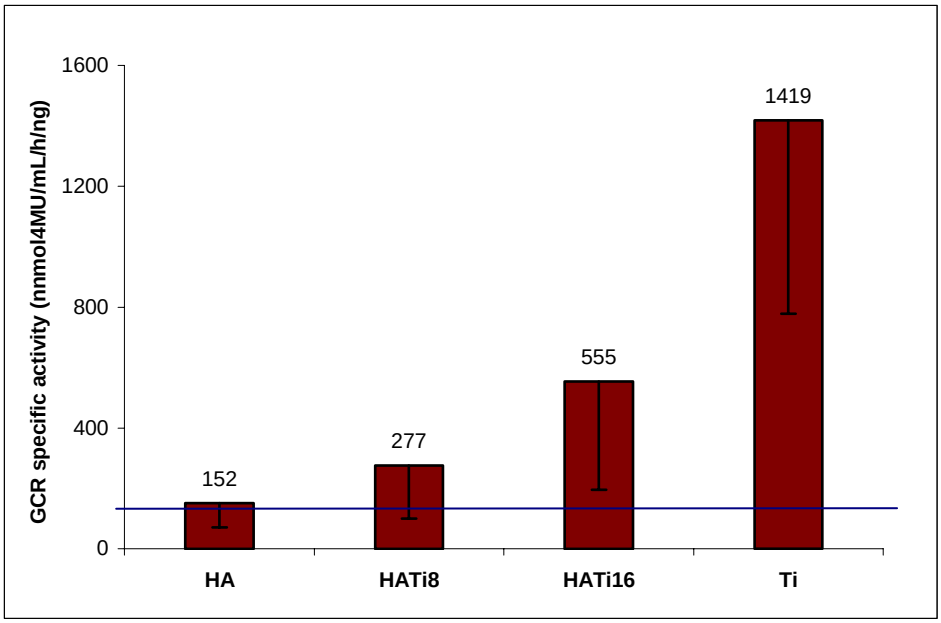

Figure 9. GCR specific activity for the different films, obtained by fluorescence spectroscopy to the reaction product 4-MU of GCR. The blue line indicates the free enzyme specific activity.

3. Conclusions

In terms of relative amount of protein that was adsorbed to each substrate, HSA and GCR behave similarly. Results showed that at pH 7.4 and for a time of incubation of 30 minutes, Ti films adsorb a higher amount of HSA and GCR per unit surface area than the other substrates (3.39 mg/m^2 and 1.88 mg/m^2, respectively). In what concerns the Ti doped films they adsorb less HSA and GCR than HA (1.77 mg/m^2 and 1.19 mg/m^2, respectively) the differences being not statistically significant for the two Ti-rich films (8 and 16%). The adsorption of HSA onto the substrates was also confirmed by IRAS and AFM techniques. AFM provided information on the distribution of the protein onto the films. Depending on the characteristics of the substrates HSA adsorbs in a more hydrated globular conformation or as a continuous film.

The activity of glucocerebrosidase adsorbed to the films was compared to the activity of the free enzyme which was used as a control. Results showed that the presence of Ti in the substrates significantly enhances the activity of the enzyme GCR.

4. References

[1] Gonçalves, IC, Martins, MC, Barbosa, MA, Ratner, BD. Protein adsorption on 18-alkil chains immobilized on hydroxyl-terminated self-assembled monolayers. Biomaterials 26 (2005): 3891-3889;

[2] Martins, MC, Ratner, BD, Barbosa, MA. Protein adsorption on mixtures of hydroxyl- and methyl-terminated alkanethiols self-assembled monolayers. J Biomed Mater Res 67 A (1) (2003): 158-171;

[3] Sa Miranda MC, Aerts JM, Pinto R, Fontes A, de Lacerda LW, van Weely S. Activity of glucocerebrosidase in extracts of different cell types from type 1 Gaucher disease patients. Clin Genet 38(3) (1990): 218-27;

[4] Holland NB, Marchant RE. Individual plasma proteins detected on rough biomaterials by phase imaging AFM. J Biomed Mater Res 51 (3) (2000): 307 – 315;

[5] Socrates, G. Infrared and Raman Characteristics Group Frequencies – Tables and Charts (3rd Ed.). John Wiley & Sons, Lda (2001), New York;

1. General Discussion and Concluding Remarks

The main objective of the present work was to contribute to the understanding of the role of titanium ions in biological processes such as protein adsorption. A particular enzyme, glucocerebrosidase (GCR), was used in the adsorption studies since previous work of our group showed that when a titanium rich calcium phosphate ($CaTi_4(PO_4)_6$) was used as a substrate, alternatively to hydroxyapatite, a higher amount of GCR per unit surface area was adsorbed and a higher catalytic activity of the enzyme was observed. Albumin adsorption studies were also performed as a control, since albumin is the protein that exists in higher concentration in plasma.

The model surfaces used as substrates in the adsorption studies consisted of sputtered films of HA, Ti, and HA doped with Ti (8 and 16% - at%).

The surface Ca/P ratio for the HA sputtered coatings has been reported to range from 1.6 to 2.6 [1-3] and it was 1.86 for the deposition conditions used in this work. Differences in Ca/P ratio between the target and sputtered coatings have been suggested to be attributed to the preferential sputtering of calcium, probably due to the possibility of the phosphorous ions being pumped away before they are deposited at the substrate [4].

It was also suggested in the literature that phosphorous ions may be weakly bound to the growing film and are sputtered away by incoming ions or electrons [5]. Another possible explanation for the Ca/P ratio being higher than the stoichiometric value of 1.67 is the fact that films include other calcium rich phase such as calcium oxide. FTIR analysis of the HA and HA doped films indicated the presence of CaO, a phase that is eliminated after washing the substrates with de-ionized water.

Coatings produced using the sputtering process, are known to be randomly deposited onto substrates as amorphous coatings [5, 6]. The as-sputtered coatings were confirmed to be amorphous by X-ray diffraction analysis. Annealing the coatings for 5 hours at 600 ºC in controlled atmosphere resulted in an increase of crystallinity only in the HA films. Doped films did not show any change in crystallinity, indicating that the presence of Ti destabilizes the HA lattice thus inhibiting its crystallization.

Various physico-chemical parameters have been shown to influence the protein adsorption on surfaces of ceramics. From a physical point of view, the morphology of

the films can influence greatly the adsorption of proteins, modulating the quantity and conformation of adsorbed proteins. For instance nanophase ceramics adsorb significantly greater quantities of vitronectin inducing an enhanced subsequent osteoblast adhesion [7, 8]. Microporosity is also an element favouring the protein adsorption in calcium phosphate ceramics since the presence of micro pores enlarges greatly the surface area of ceramics. This has been considered as an explanation of the osteoinductive potential of some ceramics after *in vivo* implantation in ectopic sites [9]. These observations highlight the importance of the physical characteristics of the ceramic films in protein adsorption studies. Although having a similar surface area, differences in the morphology were observed by AFM for the different types of substrates used in this work, an aspect that influenced the protein adsorption. For instance, it was observed that depending on the characteristics of the films, HSA adsorbed in a more hydrated globular conformation (HA doped with Ti films) or as a continuous film (HA and Ti films).

Ionic strength, pH of the medium as well as surface charge of ceramics influence protein adsorption. In the present work HA doped films are more negatively charged than HA and Ti films, and less hydrophobic, adsorbing a lower amount of protein (HSA and GCR) per unit surface area then Ti films. HA films adsorbed more HSA than doped films, but the standard deviation between the substrates was not statistically significant.

In what concerns the GCR adsorption studies, it was observed that the electrostatic characteristics of hydroxyapatite doped with titanium favours the immobilisation of GCR when compared to non doped hydroxyapatite. Although protein immobilization often results in conformational alterations that may render proteins inactive, GCR activity improved when immobilized on a substrate containing titanium. When titanium ions are present in the films a high catalytic efficiency is observed. This result is in agreement with previous studies of the group where calcium titanium phosphate was used as the substrate for GCR adsorption [10-12].

In conclusion, the results obtained indicate that titanium ions significantly influence protein adsorption and support previous suggestion of our group that calcium titanium phosphate may be used as a delivery matrix for biologically active molecules, in particular GCR.

2. References

[1] Ong JL, Lucas LC. Auger electron spectroscopy and its use for the characterization of titanium and hydroxyapatite surfaces. Biomaterials 19 (1998): 455- 64;

[2] Ong JL, Raikar GN, Smoot TM. Properties of calcium phosphate coatings before and after exposure to simulated biological fluid. Biomaterials 18 (1997): 1271-5;

[3] Hulshoff JEG. van Dijk K, de Ruitjer JE, Rietveld FJ R, Ginsel LA, Jansen JA. Interfacial phenomena: an in vitro study of the effect of calcium phosphate (Ca- P) ceramic on bone formation. J Biomed Mater Res 40 (1998): 464-74.;

[4] Zalm PC. Quantitative Sputtering. In:Cuomo JJ, Rossnagel SM, Kaufman HR, editors. Handbook of ion bearm processing technology. Park Ridge, N J: Noyes Publications (1989): 78-111;

[5] Van DijK K, Schaeken HG, Wolke JGC, Jansen JA. Inluence of annealing temperature on RF magnetron sputtered calcium phosphate coatings. Biomaterials 17 (1996): 405-410;

[6] Ong JG, Lucas LC. Post deposition heat treatment for ion beam sputter deposited calcium phosphate coatings. Biomaterials 15 (1994): 337-341;

[7] Webster TJ, Ergun C, Doremus RH, Siegel RW, Bizios R. Specific proteins mediate enhanced osteoblast adhesion on nanophase ceramics. J Biomed Mater Res 51 (2000): 475-483;

[8] Webster TJ, Schadler LS, Siegel RW, Bizios R. Mechanisms of enhanced osteoblast adhesion on nanophase alumina involve vitronectin. Tissue Engineering 7 (2001): 291-301;

[9] Yuan H, Kurashina K, de Bruijn JD, Li Y, de Groot K, Zhang X. A preliminary study on osteoinduction of two kinds of calcium phosphate ceramics - molecular clones and activites. Biomaterials 20 (1999): 1799-1806;

[10] CC Ribeiro, CC Barrias, MA Barbosa, Calcium Phosphate -alginate microspheres as enzyme delivery matrices, Biomaterials 25 (2004): 4363-4373;

[11] CC Barrias, CC Ribeiro, D Rodrigues, MC Sá Miranda, MA Barbosa, Effect of calcium phosphate addition to alginate microspheres: modulation of enzyme release kinetics and improvement of osteoblastic cell adhesion. Key Engineering Materials 284-286 (2005): 689-692;

[12] CC Barrias, CC Ribeiro, MC Martins, MA Barbosa, D Rodriguez, C Sá Miranda, Calcium phosphate microsphere for localised delivery of a therapeutic enzyme, Key Engineering Materials 309-311 (2006): 903-906.